2018-01-01

Determing Fault Location Within An Active Rift Basin Using Gravity Analysis To Determine Fault Movemnet And Effect On Water Recharge

Mark Andrew Ornelas
University of Texas at El Paso, marcornelas1003@gmail.com

DETERMING FAULT LOCATION WITHIN AN ACTIVE RIFT BASIN USING GRAVITY ANALYSIS TO DETERMINE FAULT MOVEMNET AND EFFECT ON WATER RECHARGE

MARC ANDREW ORNELAS

Master's Program in Geophysics

APPROVED:

Diane I. Doser, Ph.D., Chair

Laura Serpa, Ph.D.

Vanessa Lougheed, Ph.D.

Charles Ambler, Ph.D.
Dean of the Graduate School

Dedication

I dedicate this thesis to my mother, Maria Ornelas, for her continuing and unconditional support and sacrifice throughout my academic career. For her encouragement that never let me quit or see me fail. Thank you.

DETERMING FAULT LOCATION WITHIN AN ACTIVE RIFT BASIN USING GRAVITY ANALYSIS TO DETERMINE FAULT MOVEMNET AND EFFECT ON WATER RECHARGE

by

MARC ANDREW ORNELAS, B.S.

THESIS

Presented to the Faculty of Graduate School of

The University of Texas at El Paso

in Partial Fulfillment

of the Requirements

for the Degree of

MASTER OF SCIENCE

Department of Geological Sciences

THE UNIVERSITY OF TEXAS AT EL PASO

December 2018

Acknowledgments

I would like to first express my gratitude and appreciation to the members of my advisory committee, Dr. Diane Doser, Dr. Laura Serpa and Dr. Vanessa Lougheed. Their guidance and support through this process was unmatched and necessary to complete this journey. I would like to give a very special thanks to Dr. Diane Doser, who in all aspects of my life has provided guidance, knowledge and most importantly advice. I would like to express my sincere appreciation for her sticking with me and believing in me through both my Bachelors and Masters degrees. Without her none of this would be possible.

I would like to thank all those who assisted in field work, Jose Pablo Cervantes, Emily Graves. Your hard work and help is greatly appreciated. A special thanks to my Mother Maria Amparo Ornelas for sacrificing her Saturdays to assist in data collection just to see me succeed. Thanks to Manuel Moncada and Feliz Ziwu whom greatly assisted in data processing and map creation within this thesis. A special thanks to all my fellow graduate students who were there working side by side me and never allowed me to quit or get down . Alex Garcia, Derek Scott, Jordan Caylor, Alex Eddy and Jenna Faith.

A special thanks to UTEP staff, in particular Galen Kaip for assisting in field data collection and data processing. I would also like to thank for Carlos Montana for assisting in data processing. I would also want to thank the University of Texas at El Paso (UTEP) and the Geological Science department. I would also like to thank Mr. Joshua Viallobos, without his enthusiasm and love for geology I may have never fell in love with geology like I did. Thank you! I would also like to thank Romina Marivy Becerra Huaman, who has always guided me and stood by my side through this journey, always encouraging me to complete my graduate degree. Thanks to all

Abstract

The growth of the El Paso, TX and Ciudad Juárez, Chihuahua, metropolitan area has increased reliance of groundwater pumping from the Hueco Bolson. With growing demands for water and recharge of the bolson not occurring at a fast enough rate, water storage within the bolson is beginning to diminish. My study focuses on locating and understanding how faults interact with water flow into the basin and how they aid in storing water on the northwestern side of the bolson. Previous studies in the northernmost part of my study area have delineated a series of faults that predominantly trend northwest-southeast. In the east central part of the study area on undeveloped portions of Ft. Bliss these mapped faults begin to curve and strike north-south. Other geophysical studies in the southwest and central portions of the study area have also inferred several north-south trending faults. Gravity has shown to be a very effective geophysical method for determining fault locations in an urbanized area, and was collected with 100-500 meter spacing in areas close to the mountains where most recharge occurs and a large data gap occurs. A better determination of the fault geometry of the Hueco Bolson is crucial to understanding ground water recharge and movement within the bolson. I used the existing and newly collected gravity data, in conjunction with water well information, to analyze the relationship between fault systems and freshwater recharge and movement. In conclusion, my results displayed a strong correlation between the gravity analysis and the geochemistry of the water wells in the area. The deepening of the Hueco Bolson is still the primary factor for the diminishing water quality but the faulting creates a compartmentalization effect based on the geochemistry and gravity analysis. This compartmentalization effect, creates zones of varying water quality between north-south running faults and heading eastward the water quality decreases. Between each set of faults the wells display similar water quality and seem to be consistent in the southern and central area. The water

in the northwestern part of the study are tends to be of poorer quality likely due to the stepping over of the East Franklin Mountain Fault (EFMF).

Table of Contents

List of Figures

1. **Introduction**

El Paso, TX and its neighboring city of Ciudad Juárez, Chihuahua both rely heavily on groundwater pumped from the Hueco Bolson (Figure 1). With growing demands for water and recharge of the bolson not occurring at a fast-enough rate, water storage within the bolson is beginning to diminish. Though little can be done to increase rain fall and recharge, a better understanding of how structural and stratigraphic structures control water movement into and within the bolson will help to extend the lifetime of water within the bolson. My study focuses on locating and understanding how faults interact with water flow into the basin on the northwestern side of the bolson. This research will add to the growing database needed to ensure the best production of groundwater for the increasing demands of El Paso. For example, Marrufo (2011) proposed that the faults work as barriers in the central areas of the Hueco Bolson; however, it is unknown if these faults continue to be the primary controlling factor in the northern area of the Hueco Bolson. In Avila et al. (2016) as well as Budhathoki et al. (2018) researchers observed (based on structural cross sections they created) (Figure 2) that some faults have consistently displaced seven erosional surfaces in the same direction and have offset these surfaces by more than 30 meters. These faults are likely to have the greatest influence on groundwater movement within the bolson. In addition, some faults appear to have a complex history of differential movement that may serve as barriers to groundwater flow.

The purpose of the study is to determine the extent of several faults that have been mapped at the surface in less urbanized areas within the northwestern Hueco Bolson (Figure 3) or located in previous geophysical studies (e.g., Marrufo, 2011; Avila et al., 2016; Budhathoki 2013; Budhathoki et al., 2018) as well as to locate new faults using geophysical and water well information. My study area extends from western Ft. Bliss to the eastern edge of the Franklin

Mountains. Gravity data were collected at Ft. Bliss on a non-backed firing range that was only accessible for a short period of time in 2013. I also collected gravity data within northeastern El Paso in a large 4 km by 4 km data gap (Figure 4) in 2017. I combined these gravity data sets with gravity data from previous studies conducted by UTEP students to better trace structures as they begin to change strike from north-south to northwest-southeast in the northern basin (Figure 5).

My second objective was to create two 2-D cross sectional profiles of density variations within the study area. This will help to map the subsurface geology and create a more in-depth view of the structures controlling water flow within the study area. The profiles will aid hydrologists in modeling water flow paths and the structural and stratigraphic controls on the location of fresh and saline water within this portion of the bolson. (Figure 6).

2. Location

The study is focused on the northwestern Hueco Bolson (Figure 3). I collected gravity data in the Fort Bliss region (Area A) as well as a highly-urbanized area located east of the Franklin mountains in the northeast section of the City of El Paso (Area B) and assembled gravity data from Budhathoki (2013), Marrufo (2011), Avila (2014) and the UTEP data base (displayed as black triangles, Figure 4). A map of these data (Figure 4) shows several gaps in gravity coverage in the region closest to the Franklin Mountains (Figure 4, Area B). Yellow dots displayed on Figure 4 were collected in this study. Note they now fill some of the gravity data gaps. Area B (Figure 4) was of increased interest due to its geographical location, where recharge is occurring along range front faults and some of the freshest water is found within the Hueco Bolson. Geological and geophysical studies in the region immediately to the east of the gaps also show basin faults change trends from north-south to northwest-southeast and I would like to determine if this change in fault trends continues to the west. Therefore, the data collected in both areas A and B will help to decipher basin fault movement in the areas as well as help identify if the faults continue the north-south trends seen to the south or begin to shift to the northwest-southeast trends seen to the east.

2.2 Geology of the Area

The study area is located above the Hueco Bolson (aquifer, basin) which is a deep Tertiary/Quaternary rift basin. The Rio Grande rift has experienced two phases of extension, producing two different styles of basins (Seager et al., 1984; Morgan and Golombek, 1984). The basin is filled with unconsolidated sediments of varying clast size ranging from clay to coarse gravels, fluvial, lacustrine, and eolian sediments of Miocene to Holocene age. (Hadi, 1991; Anderholm and Heywood, 2003; Heywood and Yager, 2003; Buck et al., 1998 e.g., Marrufo, 2011; Hawley et al., 2009; Budhathoki, 2013). Geophysical studies and borehole data suggest 2500 to 3000 m of sediments fill the deepest parts of the bolson (Wen, 1983; Hadi, 1991; Collins and Raney, 1994; Hawley et al., 2009; Avila et al., 2016). Collins and Raney (1994; 2000) have mapped a series of faults within the Hueco Bolson that offset Middle Pleistocene deposits by 4 to 7 m. At least some of these faults appear to control water movement (Marrufo, 2011; Avila et al., 2016). The Franklin Mountains to the west and the Hueco Mountains to the east form the boundaries of the northern Hueco Bolson. The bolson extends southward into Northern Chihuahua, Mexico. The northern boundary is a groundwater divide which separates the Hueco Bolson and the Tularosa Basin; this divide is located just north of the Texas–New Mexico State line. Budhathoki (2018).

Early extension (mid-Oligocene to early Miocene) in the Rio Grande rift resulted in the creation of wide and relatively shallow basins with low-angle normal faults. A later extensional period (mid-Miocene to Quaternary) produced high-angle normal fault-bounded, deeper and narrower basins (Morgan and Golombek, 1984; Keller and Baldridge, 1999). Rio Grande rift extension is still occurring with evidence for a least four earthquakes along the East Franklin

Mountains fault, the fault bounding the western edge of the Hueco Bolson Aquifer, within the past 64 ky (McCalpin, 2006).

3. Previous Studies

3.1 Geological Studies:

The Hueco Bolson is part of a series of interconnected grabens which forms the Rio Grande rift system that extends from Colorado to west Texas (Figure 7). The Hueco Bolson contains two subbasins, and the northern is the focus of this study. The northern section of the bolson appears to have developed later in the Quaternary than the southern section of the bolson. The youngest faulting (< 17,000 years ago, McCalpin, 2006) is found along the East Franklin Mountains fault within the northern bolson. Faults in the northern bolson tend to strike north-south, while those in the southern bolson strike northwest-southeast. This likely reflects the change of stress directions during the history of Quaternary extension in the region.

Fill in the Hueco Bolson is primarily composed of Oligocene to Holocene lacustrine and eolian sediments. These sediments can be divided into Tertiary lower basin fill, Tertiary-Quaternary upper basin fill and surficial deposits (Collins and Raney, 1994). The surface deposits consist of windblown sand, Rio Grande and arroyo alluvium, and alluvial fans as well as other gravel units (Collins and Raney, 1994).

Seager (1980) characterizes the northwest section of the Hueco Bolson as an asymmetric, west tilted graben. Ramberg et al. (1978) have also described the asymmetry of the bolson and estimated a maximum fill thickness of between 2000 m to 3000 m. The deepest section of the Bolson is bounded by major faults as described by Collins and Raney (1994). The Eastern Franklin Mountains fault along the western edge of the basin shows the greatest amount of offset (~ 120 m), however Collins and Raney (1994) have mapped a series of Quaternary faults having offsets of ~4 to ~8 m throughout the basin

In previous work in the area by Hawley et al. (2009), Marrufo (2011) and Budhathoki (2013) well logs and cuttings were utilized to develop more detailed stratigraphy and upper basin structure. They used grain size analysis and well log analysis to better describe the stratigraphy and basin structure at depth. The well logs consisted of natural gamma ray, resistivity and spontaneous potential logs. Their results all indicate more faults are present within the bolson than those seen and mapped at surface. These results may seem surprising, but due to highly-urbanized nature of the study area fault scarps or other surface features related to the faulting were likely obliterated when the region underwent development.

3.2 Geophysical Studies:

Urbanization limits our ability to use geophysical techniques within the basin. Some seismic reflection (see Collins and Raney, 1994; Figuers, 1987) and electromagnetic studies (Paine and Collins, 2017) have been conducted at the less urbanized edges of the northern basin and in the southern subbasin, but most work in the northern subbasin has been focused on gravity and well log studies (Avila et al., 2016; Budhathoki et al., 2018; Marrufo, 2011).

Gravity studies take advantage of the fact that materials of differing density are offset across a fault, so that a change in gravitational attraction is seen when crossing a fault. As depth to basement increases within the bolson, the amount of less dense sediment increases, also affecting gravity readings. Several geophysical techniques can achieve similar results and take advantage of varying changes in the subsurface. Similar studies around the world have used gravity, seismic and resistivity among other geophysical methods to understand subsurface geology. Specifically, Gabtni et al. (2012), Martinez et al. (2017) and Soupios et al. (2007) investigated similar areas, involving the understanding of subsurface structures. Martinez et al. (2017) used deep resistivity soundings and time domain electromagnetics to map possible

intrusions of sea water into fresh water aquifers within a semiarid region of Portugal. The resistivity soundings are able to detect the high contrast between the fresh and saltwater and geological layers within the aquifer. Gabtni et al. (2012) used land and satellite gravity readings as well as seismic reflection profiles to map the subsurface structure of the Jeffara Basin region in Tunisia, Africa. Soupios et al. (2007) utilized surface resistivity soundings and correlated them to calculate borehole resistivity. This was used to estimate aquifer parameters which is crucial in the area for water resource management. Gabtni et al. (2012), Martinez et al. (2017) and Soupios et al. (2007) all had great success in imaging the subsurface and understanding the extent and structures in these basin systems. These areas are arid to semiarid, similar to where my study is taking place. These studies reinforce the need to use geophysics to better understand subsurface controls to assist in managing water resources.

In the northernmost part of my study area Budhathoki et al. (2018) used gravity data to delineate a series of faults (brown lines, Figure 5) that predominantly trend northwest-southeast. Some of these faults appear to be extensions of faults mapped by Collins and Raney (2000) (white lines, Figure 5) into more urbanized areas where the faults could not be observed at the surface. In the east central part of the study area on undeveloped portions of Ft. Bliss, Collins and Raney (2000) indicate these faults begin to curve and strike north-south. Avila et al. (2016) and Budhathoki et al. (2018) conducted several microgravity surveys in the northeastern part of El Paso and were able to detect nearly all the faults within their study areas that had been previously mapped by Collins and Raney (2000). Avila et al. (2016) used the Horizontal Gradient Magnitude (HGM) method to successfully extend a number of previously mapped north-south striking faults of Collins and Raney (2000) into the urbanized areas of central El Paso. Marrufo (2011) used

gravity and well log information to suggest that a north-south striking fault was located between the East Franklin Mountains fault and faults mapped by Collins and Raney (Figure 5, fault M1) that appears to form the western edge of the deepest part of the basin (bedrock depths > 2 km). Due to lack of gravity data within Area B (Figure 4) we do not know if faults with similar north-south trends exist in this region or if the trends of faults begin to change to strike northwest-southeast. Since Area B contains some of the freshest water within the bolson (Hutchison, 2004), an understanding of how faults within this region direct or block water flow is crucial. In this study, I collected microgravity and water well information in an effort to better understand the structure and stratigraphy within this important portion of the aquifer.

4. Methodology and Data Processing

4.1 Gravity Collection

The use of gravity analysis has been proven to be incredibly helpful in determining fault location within the Hueco Bolson (Marrufo, 2011; Budhathoki et al., 2016; Avila et al., 2016). Figure 4 shows the gravity data amassed by UTEP in the area as black triangles. The yellow circles represent the data I collected. These new data were crucial determining the extent of several faults mapped in both areas. (Collins and Raney 2000; Marrufo, 2011; Budhathoki et al., 2018; Avila et al., 2016).

Each survey presented several hurtles. Area A (Figure 4) is located on an unbacked shooting range on Fort Bliss and is utilized for several types of training including using live ammunition of varying calibers. This made accessibility nearly impossible. However, a pre-planned closure of this region due to some improvement and maintenance of existing utilities in the area allowed access. Area B (Figure 4) was a heavily urbanized section of the city that presented collection difficulties due to heavy traffic of many sorts.

For this study 256 gravity points were collected in two separate areas. (Figure 4) To insure dense enough coverage to detect faults within area A, gravity data were collected by Galen Kaip and me using a grid with station spacing varying from 100 to 500 meters (Figure 4). I also created a grid sampling plan for Area B with spacing varying between 250 and 500 meters. Because this region is more urbanized than area A, more flexibility was needed in the data collection process. Data in this region were collected by Emily Graves and me.

We utilized a Lacoste-Romberg model G-115 gravimeter with microGal precision in this study. To ensure proper location and elevation of each station we employed a highly accurate Topcon GB-1000 differential GPS. We submitted the GPS data points to OPUS, an online

Positioning User Service. OPUS processes the GPS points with respect to three reference points and the processed points are then returned to the user. The data points are then reprocessed using the solution formulated by OPUS. This is used to ensure a high level of accuracy on elevation estimates (to within 5 cm) and also the corresponding latitude and longitude.

We used a previously created base station by Budhathoki (2013) as the primary base station. We collected the gravity points in loops of varying time lengths between 2-3 hours. Returning to the base station frequently reduces the effects of tide and instrument drift. To ensure accuracy at the beginning and end of every collection day we took a gravity reading at the Kidd Memorial Seismological Observatory, an absolute gravity base station located on the UTEP campus.

I then converted the collected gravity data from dial units to gravity units and performed standard corrections to the gravity data including tide, drift, free air, terrain and Bouguer. Next I integrated these data with existing data to create a series of maps (complete Bouguer, residual Bouguer, horizontal gradient magnitude) to help determine fault locations. Finally, I constructed a series of 2-D density profiles using available water well and geophysical information to better image subsurface structure and its effect on water quality.

4.1.1 Drift Correction

The Lacoste and Romberg instrument utilized in this study is affected by drift, which is caused by varying temperatures, pressures and the Earth's tides. This is counteracted by returning to a gravity base in the area over a period of time, usually 3 hours. This allows me to perform a linear estimate of drift per minute.

4.1.2 Free Air Correction

Gravity readings decrease as the distance between masses increases. The free air correction solely considers the change in gravity with distance from the center of the earth. For this reason, it is necessary to correct the reading due to elevation changes observed at each station and reduce the readings to a common reference level.

4.1.3 Bouguer Correction

The Bouguer correction corrects for the attraction of material between the station and the datum plane which was previously ignored in the free-air correction (Telford et al., 1990). The correction assumes a horizontally infinite slab of constant density. For my calculations I assumed a slab density of 2670 g/cm^3

4.1.4 Terrain Correction

Terrain corrections were used in order to remove the effects of topographic features within or near the study area. A Digital Elevation Model (DEM) was utilized to correct for the effect of these features. The terrain correction was needed to produce the Complete Bouguer Anomaly map (Figure 8)

4.2 GPS Processing

The GPS data collected for the study was acquired by using a *Topcon GB-1000* differential GPS, which has a vertical accuracy as low as 1cm. A static mode survey was implemented, which

uses a fixed location (base) and a roving unit (rover) for the survey. The fixed receiver was placed at the same position as the base station (Figure 4). A static survey collected in kinematic mode was utilized due to the actual survey grid spacing between each gravity reading. When beginning the survey, the first GPS readings collected on each field day were based on the data collected in a 600 second (10 minutes) period in the same location as the base station in order to achieve excellent pairing of the base and rover units. The subsequent data points were collected with 180 to 360 seconds of GPS data. Though the use of static survey gives greater accuracy than a kinematic survey, the accuracy given with a kinematic survey was sufficient for the GPS portion of the study.

The gravity data were collected over several weeks due to the complexity of accessing the urban areas and the rugged terrain of the unurbanized area. The resulting data were transferred from the Topcon GB-100 differential GPS base and rover to an excel sheet to be merged with other collected sets as well as for further processing. After all the data were collected, the data from the fixed base station were sent in to Online Positioning User Service or OPUS. OPUS creates a solution which helps to better locate the base station and provided accuracy within a centimeter of error. The solution is then applied to the roving data and locations are modified to reflect the corrected base location and increased accuracy. The data were then uploaded to the UTEP gravity database.

5. Results and Discussion

5.1 Gravity Data Processing

Minimum curvature was the primary method used for data interpolation. Minimum curvature was utilized to create the smoothest surface from the data, as we expect the data values to vary slowly over the study area. When integrating the newly collected data to the existing data maintaining accuracy was crucial. Comparisons between Bouguer gravity anomaly data obtained from points collected at the edges of the study areas (collected both from this survey and previous surveys) was conducted and the accuracy was between 0.05 and 1 mGal.

5.2 Gravity interpretation

5.2.1 Complete Bouguer Anomaly

The collection of gravity points within Area A and B allowed for more detail to be seen and detect changes within the geology of the Hueco bolson at depth (Figure 8). The map indicates the deepening of the Bolson to the east following known geologic features and regional trends. The gravity anomaly increases to the west as it approaches the edge of the Franklin Mountains. In the southwestern portion of the study area the complete Bouguer anomaly map primarily shows north-south trending contours. This pattern suggests a series of faults stepping down to the deepest part of the basin rather than a great amount of offset along one fault. Towards the central and western part of the study area gravity anomaly contours begin to trend northeast-southwest while

in the eastern portion of the study area the dominant trend in the contours disappears. The lowest anomaly values are observed in the extreme northeastern part of the study are (Figure 8).

5.3 Data Modeling

In order to illustrate the changes seen within the gravity, the final step was to create various density cross-sections profiles. (Figure 9 and 10) The location of these cross-section was chosen strategically to include several water wells in the area (Figure 6). This was crucial to help constrain the geology at depth as well as increase the understanding of the fault interaction with water chemistry as best as possible. Several previous studies (Avila et al., 2016; Budhathoki et al., 2018; Collins and Raney, 1994; Hawley et al., 2009) helped constrain the density models as well. Both density profiles were selected to run east-west to increase the chance of crossing faults, which predominately run north-south and northwest-southeast within the bolson. Figure 2 shows two cross sections C-C' from Avila et al. (2016) and B-B' from Budhathoki (2016). Both cross-sections show high angle normal faults that create a step-down feature as the bolson deepens.

The Density profiles were created using GM-SYS^{TM} forward modeling software which works with Oasis Montaj ^{TM}. The forward modeling technique is based on the Talwani 2.5D modeling approach of Talwani and Heirtzler (1964) and Talwani et al. (1959). To model the profiles I created series of polygons based on known and assumed geology that were each assigned a density value. My densities were based on values from Avila et al. (2016). The software then calculated a gravity response based on the polygons and densities. I then compared observed and the calculated values of gravity and adjusted my models so that a reasonable error was found that did not violate known geologic constraints. I used three polygons in my

modeling. These were (from surface to depth): Upper basin fill (D=2100 kg/m^3), lower basin fill (D=2300 kg/m^3) and Precambrian basement (D=2700 kg/m^3).

5.3.1 Profile A-A'

Profile A-A' is the southern density profile shown in Figure 9, the profile follows the northernmost line of data collected in area B and then the southernmost line of data collected in area A. The profile also includes gravity data from Marrufo (2011) (Figure 4). A-A' was placed in this location to use well information from wells 025A, 27A and 601 (Figure 6). Not only was information from these wells used to constrain the profiles, but I compared water geochemistry changes in these wells to my modeled basin structure. Profile A-A' crosses 3 previously mapped faults, two surface faults from Collins and Raney (1994) (faults X, IX) as well as a geophysically referenced fault (M1) located by Marrufo (2011).

The complete Bouguer anomaly map (Figure 8) shows highs on the western side of the profile and decreases to the east through the profile (Figure 8). A total difference of 18 mGals is observed over the length of the profile. To match the gravity anomaly high seen in the west I added a body consistent with the density of the Franklin Mountains. I then added the three known faults that lie along the profile with throws and orientations consistent with previous research results. The model generated had a very high error (rms error of 4.2 mGal); this indicated the need for further changes and the need to add additional structures to better represent the geology at depth. I next extended faults had been mapped to the north (e.g. Budhathoki et al., 2018) into the model and I adjusted the model to accommodate these faults,

again preserving the same directions of throw and orientation as observed to the north. The model error was significantly reduced (rms error of 0.56 mGal) by extending faults 30 and XVI (Figure 11) to the south. The faults also correlate well with the observed trends and changes in the contours observed in the complete Bouguer anomaly map (Figure 8).

5.3.2 Profile B-B'

Profile B-B' is the northern density profile line (Figure 10). It includes gravity data from Area A as well as data collected by Budhathoki (2016). B-B' was placed in this location to use water well information from wells 31, 29B, 40A, 521, and FBT04 (Figure 6). The profile crosses four previously mapped surface faults from Collins and Raney (1994) (faults VII, VIII, IX, X). These four faults were the first structures I introduced into the density model. Faults XVI and 30 also had to be incorporated into my density model to better match the observations and reduce error. However, the error was still relatively high (rms error of 3.64 mGals) and some deepening of the basin as well as variation in the amount of throw across faults had to be changed to produce a lower amount of error (2.12 mGals). Finally, I introduced another fault into the model to further lower error. I noticed that fault M1 was the only previously mapped fault in the region that could possibly be extended to the north and intersect my profile line. By introducing this fault I achieved an rms error of 0.531 mGal. Note that the extension of fault M1 correlates well with contours observed in the Complete Bouguer anomaly map (Figure 11). B-B' also displays a change in the character of EFMF. This may be due to a step over which is occurring to the north. It is likely that EFMF is no longer fault with greatest offset in this region.

Both of my density profiles supported the deepening of the rift towards the east and the predominance of north-south trending faults within the study area. I next compared the location of faults from my models to changes in water quality across the study area.

5.4 Geochemistry

Faults often serve as barriers or conduits to the flow of water in basins. In order to determine how the faults might control water quality (i.e., Total Dissolved Solids (TDS), chloride-sulfate (Cl/SO_4) ratios) Thapalia (2014) gathered data for 45 water wells from the EPWU (El Paso Water Utilities) (see Table 1 appendix). Sampling interval depths, TDS, Ca,Na,Cl,SO_4 and pH were available for 35 of the wells. The remaining 10 wells only had TDS values.

Thapalia (2014) first subdivided the wells based on their proximity to the Franklin Mountains. She termed one group of wells mountain front wells (MF) and the other central basin wells (CB) (Figure 12). She suggested that MF wells would be more likely to have higher quality water since they would be better positioned to receive recharge from mountain precipitation. She then further subdivided the wells based on their Cl/SO_4 ratios into 4 descending categories (12:1, 4:1, 1.5:1, and 1:2) with water quality improving as the ratio lessens. Figure 13 illustrates how ratios are primarily grouped into distinct areas of the bolson. Overall the ratios increase (higher salinity) as the bolson deepens but there are several areas where the water quality does not match the location of the well with respect to the mountain front (Figure 13). To further understand this pattern, TDS values for all 45 wells, as well as fault

locations were plotted (Figure 14) to illustrate relationships between water chemistry and faults

In both figures a general compartmentalization effect can be seen. Figure 13 indicates that in the central and southern part of my study area fault 30 separates wells with Cl/SO_4 ratios of 1:2 (best water) from ratios of 1.5:1. Fault M1 appears to separate wells with Cl/SO_4 ratios of 1.5:1 from ratios of 4:1. This would suggest that faults 30 and M1 serve as barriers to water flow in this part of the bolson.

These patterns break down in the northern part of my study area, suggesting that the change in strike of faults within this area as well as the termination of some faults may create pathways for more water mixing. Note that the highest Cl/SO_4 ratios (12:1) are found in two wells near the mountain front in the northern part of my study area as well as near the northern extension of fault 10 (Figure 13). The two mountain front wells are located within a region where the East Franklin Mountains fault steps 2-3 km westward along the mountain front. Regions of fault step overs can be highly fractured and could allow upwelling of poorer quality, deeper basin water as well as differential uplift of deeper, more saline, playa sediments as suggested by Budhathoki et al. (2018).

Figure 14 compares TDS (size of circle) to sampling depth (color of circle) for my study area. Note that the white symbols indicate wells where sampling depths were not available. In general TDS values increase to the east, but also to the north. These trends are similar to those observed for changes in the Cl/SO_4 ratios. I also note that there are significant changes in TDS values across fault 30 (from less than 440 to 440-713 ppm) (similar to the Cl/SO_4 ratios).

However, fault XVI appears to act as a barrier dividing water of 440-713 ppm from 718-1224 ppm while I do not observe a major change in TDS across fault M1.

Although we might expect TDS to increase with well depth since more lacustrine and playa lake facies with higher amounts of evaporites are found with increasing depth (Budhathoki et al., 2018), this trend is not observed. Rather, it appears that high TDS values are found at sampling depths of 101-120 m (Figure 15). One difficulty of comparing both the Cl/SO_4 ratios and TDS values to sampling depth is that in many cases the EPWU reported TDS for a large sampling interval (50-100 m) that reflects mixing of water from several aquifer units of varying quality.

A similar compartmentalization of wells occurs between fault 30 and XVI with a water quality trend that stays consistent with the first set of wells in the southern section west of fault 30. A total of 12 wells lie in this area, all but one show 1.5:1 $Cl/S0_4$ ratios (blue diamonds, Figure 13), and to the north a single well shows a 12:1 Cl/SO_4 ratio (red crosses, Figure 13). The TDS values show a similar trend, with all 11 wells extracting from moderately deep sampling depths ~80-120 m and a single well to the south having a sampling depth of ~181+ m (Figure 15). Ten of the 11 wells all have similar TDS values with good to moderately good quality water, between 258-1224 TDS. A single well to the north-northeast lying just east of the mapped location of fault 30 has poorer quality water ~2389 +TDS and a 12:1 Cl/SO_4 ratio.

Similar compartmentalization occur as the bolson deepens easterly; between faults XVI and M1 lie 4 wells with known TDS and Cl/SO_4 ratios. All have similar TDS values (718-2389)

but a wider range of sampling depths between 80-160 meters. Three of the four show 1.5:1 Cl/SO_4 ratios and the single outlier has 4:1 Cl/ SO_4 ratio. (Figure 14 and 15). To the east of fault M1 lie 5 wells with known TDS and Cl/ SO_4 ratios, three of the four have ratios of 4:1 and one has a 1.5:1 Cl/ SO_4 ratios. All have similar TDS values (718-2389) but the widest range of sampling depths from 80 to 181+ meters. Farther east, the remaining wells lack sampling depth and Cl/ SO_4 ratio information, but did include TDS levels. Though the TDS values come from unknown depths all values are higher than the wells that lie to the west within the above explained zones.

As the bolson deepens to the east from the edge of the Franklin Mountains the water quality begins to decrease as supported by both Cl/SO_4 ratios and TDS values. Other than a few wells to the north, most follow a trend of similar values TDS values and Cl/ SO_4 ratios, but with greatly varying sampling depths. The faults I propose to extend through my study area seem to compartmentalize these zones of water quality and support the observation that the water quality decreases as the Bolson deepens, with the faults having some degree of influence on water quality. For the several wells that lacked sampling depths and Cl/ SO_4 ratios we can hypothesize that they may also be similarly affected by fault structure. If geochemical data could be obtained for these wells I could better determine the overall role of intrabasin faults in compartmentalizing water quality.

6. Conclusion

The Hueco Bolson is a critical aquifer for the El Paso area. The lack of precipitation in our region, as well as declining snowpack in the headwaters of the Rio Grande, results in reduced availability of surface water. This cumulative effect increases our dependency on ground water in the future. A detailed study of the possible structural controls of the Hueco Bolson aquifer system can help predict where the best quality water may be found for future development. This study incorporates geophysical and geochemical techniques which may help to close the knowledge gap and demonstrates the usefulness of using gravity studies in highly urbanized regions where other geophysical methods might be difficult to conduct.

This research improved our understanding of the fault networks within the northwestern Hueco Bolson. Faults in my study area are characterized by a predominately north-south trend. The gravity analysis suggests we can extend faults 30 and XVI to the south of previous studies (e.g., Budhathoki et al., 2018) and fault M1 (e.g. Avila et al., 2016) to the north. Density profile B-B' also suggests that the character of Eastern Franklin Mountain Fault (EFMF) changes to the north of Transmountain Drive where it steps over about 3 km to the west. In this region a greater amount of offset may be taking up on other intrabasin faults.

Comparison of geochemistry data to gravity modeling results suggests that north-south trending faults in southern and central part of my study area serve as barriers to flow and appear to compartmentalize different qualities of water. More detailed analysis of this compartmentalization is hampered by the fact that some geochemical data represent a mixture of

waters from different units within the aquifer system.

North of my study area some faults begin to strike to the northwest (Budhathoki et al., 2018) and others appear to terminate such as faults M1 and IX. The change in water chemistry to the north of my study area suggests that in this region the termination of faults or changes in strike direction may allow the faults to act as conduits that bring up deeper, poorer quality water. In addition, the stepover of the EFMF to the west has likely caused fracturing of the hanging wall block which may create or increase upwelling of deeper, poorer quality waters. The stepover might also have led to differential uplift of the deeper Santa Fe formation that contains poorer quality water.

This study demonstrates the value of using geophysics to investigate areas where future water wells may be drilled to provide a baseline idea of basin fault networks and their possible control on ground water flow and quality. The gravity method can cover a broad area for a relatively low cost, especially in areas where urbanization may make the use of other techniques difficult. In regions where human made features are less likely to interfere with other geophysical methods, electrical and magnetic methods may also be cost effective to combine with gravity studies. Regardless of the geophysical techniques applied, these methods will aid in the planning and development of future aquifers within west Texas.

Within the Hueco Bolson collection of additional gravity data in the region of where the EFMFZ steps over would aid in determining the structural controls might lead to the occurrence of such poor quality water at the mountain front. Collection of data in the eastern bolson would

provide more details on the shape of this portion of the bolson. Although water quality is very poor in the eastern bolson, an increased knowledge of fault structure and basin structure is necessary to develop models of shaking expected in a future large earthquake along the EFMF.

References

Anderholm, S.K., and Heywood, C.E., 2003, Chemistry and Age of Ground Water in the Southwestern Hueco Bolson, New Mexico and Texas: U.S. Geological Survey Water-Resources Investigations Report 02–4237, 16p.

Avila, V.M., Doser, D.I., Dena-Ornelas, O.S., Moncada, M.M., and Marrufo-Cannon, S.S., 2016, Using geophysical techniques to trace active faults in the urbanized northern Hueco Bolson, West Texas, USA, and northern Chihuahua, Mexico: Geosphere 12, p. 264-280, GES01228.1, doi: 10.1130/GES01228.1.

Avila, V.M., 2016, Geophysical constraints on the Hueco and Mesilla Bolson: Structure and Geometry [Ph.D. thesis]: El Paso, University of Texas at El Paso, 90 p.

Avila, V. M., 2011, An investigation of the seismic hazards of the El Paso-Juarez region: the nature and extent of the southern east Franklin mountains fault zone [M.S. thesis]: El Paso, University of Texas at El Paso, 51 p.

Budhathoki, p., 2013, Integrated geological and geophysical studies of the Indio Mountains and Hueco Bolson, West Texas [Ph.D. thesis]: El Paso, University of Texas and El Paso, 126 p.

Burgos, A., 1993, A gravimetric study of the thickness of the unconsolidated materials in the Hueco Bolson aquifer, Juarez area, Chihuahua Mexico [M.S. thesis]: El Paso, University of Texas at El Paso, 259 p.

Collins, E.W., and Raney, J.A., 2000, Geologic map of west Hueco Bolson, El Paso region, Texas: Miscellaneous Map No. 40, Texas Bureau Econ. Geol., 1 sheet, scale 1: 100,000.

Collins, E.W., and Raney, J.A., 1994, Tertiary and Quaternary tectonics of the Hueco bolson, Trans-Pecos Texas and Chihuahua Mexico, *in* Keller, G.R., and Cather, S.M., eds., Basins of the Rio Grande Rift: Structure, Stratigraphy, and Tectonic Setting: Boulder, CO, Geol. Soc. Amer. Spec. Paper 291, p. 265-282.

Gabtni, H., Alyahyaoui, S., Jallouli, C., & Hasni, W., and Mickus, K., 2012, Gravity and seismic reflection imaging of a deep aquifer in an arid region: Case history from the Jeffara basin, southeastern Tunisia. Journal of African Earth Sciences, v. 66–67, p.85–97. 10.1016/j.jafrearsci.2012.03.007.

Hadi, J., 1991. A Study of the structure and subsurface geometry of the Hueco Bolson [M.S. thesis]: El Paso, University of Texas at El Paso, 88 p.

Hawley, J.W., Kennedy, J.R., Granados-Olivas, A., and Ortiz, M.A., 2009, Hydrologic Framework of the Binational Western Hueco Bolson-Paso del Norte Area, Texas, New Mexico and

Chihuahua: Overview and Progress Report on Digital-Model Development, WRRI Tech. Compl. Rept. 349, 45 p.

Heywood, C.E., and Yager, R.M., 2003, Simulated Ground-Water Flow in the Hueco Bolson, an Alluvial-Basin Aquifer System near El Paso, Texas: U.S. Geological Survey Water-Resources Investigations Report 02–4108, 55p.

Hutchison, R., 2004, Hueco Bolson Groundwater Conditions and Management Report: http://www.epwu.org/water/hueco_bolson.html (accessed 15 July 2016).

Keller, G.R., and Baldridge, W.S., 1999, The Rio Grande rift: A geological and geophysical overview: Rocky Mountain Geology, v. 34, p. 121–130, https://doi.org/10.2113/34.1.121.

Marrufo, S. S., 2011, An integrated geological and geophysical study of the fresh and brackish water boundary in the Hueco Bolson, west Texas [M.S. thesis]: El Paso, University of Texas at El Paso, 108 p.

Martínez-Moreno, F. & Monteiro-Santos, F.A. & Bernardo, I & Farzamian, M. & Nascimento, C. & Fernandes, J. & Casal, B. & Ribeiro, J. (2017). Identifying seawater intrusion in coastal areas by means of 1D and quasi–2D joint inversion of TDEM and VES data. Journal of Hydrology. 552. 10.1016/j.jhydrol.2017.07.026.

McCalpin, J.P., 2006, Quaternary Faulting and Seismic Source Characterization in the El Paso–Juarez Metropolitan Area: Final Technical Report: Collaborative Research with the University of Texas at El Paso, Program Element II: Evaluate Urban Hazard and Risk, and National Earthquake Hazards Reduction Program, U.S. Geological Survey, 68 p., http://geohaz.com/images/document-map-downloads/contract-rpts/geo-haz_2006-E-Franklin-fault-TX-LowRes.pdf

Morgan, P., and Golombek, M.P., 1984, Factors controlling the phases and styles of extension in the northern Rio Grande rift*, in* Baldridge, W.A., Dickerson, P.W., Riecker, R.E., and Zidek, J., eds., New Mexico Geological Society 35th Field Conference Guidebook: Socorro, New Mexico, New Mexico Geological Society, p. 13–19.

Seager, W.R., Shafiqullah, M., Hawley, J.W., and Marvin, R.F., 1984, New K-Ar dates from basalts and the evolution of the southern Rio Grande: Geological Society of America Bulletin, v. 95, p. 87-99, https://doi.org/10.1130/00167606(1984)95<87:NKDFBA>2.0.CO;2.

Soupios, P. & Kouli, M. & Vallianatos, F. & Vafidis, A. & Stavroulakis, G., 2007. Estimation of aquifer hydraulic parameters from surficial geophysical methods: A case study of Keritis Basin in Chania (Crete – Greece). Journal of Hydrology. 338. 122-131. 10.1016/j.jhydrol.2007.02.028.

Talwani, M., Worzel, J.L., and Landisman, M., 1959, Rapid gravity computations for two-dimensional bodies with application to the Mendocino submarine fracture zone: Journal of Geophysical Research, 64, no. 1, p. 49–59, doi: 10.1029/JZ064i001p00049.

Talwani, M., and Heirtzler, J.R., 1964. Computation of magnetic anomalies caused by two-dimensional structures of arbitrary shape, computers in the mineral industries: School of Earth Sciences, Stanford University (Publication), p. 464-480.

Thapalia, A., 2014, Geochemical studies of backfill aggregate, lake sediment cores and the Hueco Bolson Aquifer [Ph.D. thesis]: El Paso, University of Texas and El Paso, 142 p.

Wen, D.E. (1983) Summary of Hydrologic Information in the El Paso TX area. U.SG.S. Open File Report 83-775, 77 p.

US Geological Survey, Quaternary Faults map, USGS Geologic Hazards Science Center Golden CO. https://usgs.maps.arcgis.com/apps/webappviewer/index. Last accessed, December 2018

Appendix

Table 1

State No.	Well No.	Lat	Long	Sampling Dates	Sampling intervals	Ca	Na	Cl	SO4	TDS	pH
JL-4905-321	LF1	31.98608	-106.4094379	1988-2009	300-500	76.95	250.26	178.89	435.58	1224.83	7.65
JL-4905-325	LF4	32.00101	-106.4094148	1989-2013	300-500	24.75	52.81	29.09	47.88	258.37	8.02
JL-4905-305	E5	31.98594	-106.4119439	1965-2010	374-499	30.21	78.27	87.03	48.04	347.91	7.98
JL-4905-305	E5	31.98594	-106.4119439	n/a	n/a	n/a	n/a	n/a	n/a	814	n/a
JL-4905-305	E5	31.98594	-106.4119439	n/a	n/a	n/a	n/a	n/a	n/a	3899	n/a
JL-4905-212	E6	32.00095	-106.4260956	1974-2013	463-839	42.6	101.87	157.27	41.63	459.4	7.97
JL-4905-212	E6	32.00095	-106.4260956	1974-2013	463-839	42.6	101.87	157.27	41.63	459.4	7.97
JL-4905-213	E7	32.00099	-106.4175455	1975-2008	445-875	49.77	160.19	271.5	41.34	643.27	7.92
JL-4905-213	E7	32.00099	-106.4175455	1975-2009	445-875	49.77	160.19	271.5	41.34	643.27	7.92
n/a	E3A	32.0001	-106.432976	n/a	n/a	n/a	n/a	n/a	n/a	631	n/a
n/a	E3A	32.0001	-106.432976	n/a	n/a	n/a	n/a	n/a	n/a	663	n/a
JL_4905-804	24	31.88494	-106.4229338	1952-2002	301-788	49.03	64.37	65.57	60.51	416.38	7.9
JL-4905-811	024A	31.88494	-106.4229338	2004-2013	650-885	53.53	91.09	82.3	73.46	454.29	7.59
JL-4905-803	025A	31.90076	-106.4224575	1953-2013	318-428	48.13	91.4	95.21	73.73	492.25	7.8
JL-4905-802	26	31.913	-106.424	1953-2012	360-820	46.27	112.2	129.31	81.07	555.67	7.87
JL-4905-802	26	31.913	-106.424	1953-2012	360-820	46.27	112.2	129.31	81.07	555.67	7.87

JL-4905-902	27	31.89994	-106.4103269	1955-1990	360-832	34.58	141.97	132.67	89.23	548.61	7.95
JL-4905-902	27A	31.89994	-106.4103269	2002-2013	680-700	81.73	281.64	456.74	95.23	1138.14	7.74
JL-4905-902	27A	31.89994	-106.4103269	2002-2013	680-800	n/a	n/a	n/a	n/a	1330	n/a
JL-4905-902	27A	31.89994	-106.4103269	2002-2013	880-1000	n/a	n/a	n/a	n/a	3040	n/a
JL-4905-901	28	31.91362	-106.4078754	1956-2013	348-727	32.66	110.28	89.06	81.96	475.42	8.03
JL-4905-901	28	31.91362	-106.4078754	1956-2013	348-727	32.66	110.28	89.06	81.96	475.42	8.03
JL-4905-606	29	31.92815	-106.4064247	1956-1980	310-766	32.05	123.52	114.76	82.19	493.86	8.09
JL-4905-615	29A	31.92815	-106.4064247	1982-1996	557-920	33.16	121.79	144.95	60.95	491.95	8.01
JL-4905-615	29B	31.92815	-106.4064247	2005-2013	550-1020	36.48	131.89	190.56	63.17	519.67	7.79
JL-4905-615	29B	31.92815	-106.4064247	2005-2013	550-1020	36.48	131.89	190.56	63.17	519.67	7.79
JL-4905-615	29B	31.92815	-106.4064247	2005-2013	550-1020	n/a	n/a	n/a	n/a	791	n/a
JL-4905-501	31	31.92775	-106.4253123	1957-2007	319-730	35.83	110.98	96.07	69.71	489.25	7.9
JL-4905-501	31	31.92775	-106.4253123	1957-2007	319-730	35.83	110.98	96.07	69.71	489.25	7.9
JL-4905-603	32	31.94239	-106.4085982	1957-2010	335-657	32.45	106.42	95.69	72.83	450.79	8
JL-4905-603	32	31.94239	-106.4085982	1957-2010	335-657	32.45	106.42	95.69	72.83	450.79	8
JL-4905-801	33	31.91401	-106.4405387	1957-2013	418-1125	37.13	68.39	36.35	44.16	368.44	7.76
JL-4905-801	33	31.91401	-106.4405387	1957-2013	418-1125	37.13	68.39	36.35	44.16	368.44	7.76
JL-4905-801	33	31.91401	-106.4405387	1957-2013	418-1125	37.13	68.39	36.35	44.16	368.44	7.76
JL-4905-604	34	31.94376	-106.3918717	1958-2007	325-802	55.07	100.98	153.2	82.41	512.63	8.07
JL-4905-604	34	31.94376	-106.3918717	1958-2007	325-802	55.07	100.98	153.2	82.41	512.63	8.07
JL-4905-602	35	31.95725	-106.3921736	1958-2009	354-699	119.05	165.49	317	169.15	942.55	7.82
JL-4905-602	35	31.95725	-106.3921736	1958-2009	354-699	119.05	165.49	317	169.15	942.55	7.82
JL-4905-601	36A	31.95697	-106.4073405	1958-2007	350-690	43	106.14	109.12	94.24	502.35	7.94
JL-4905-601	36A	31.95697	-106.4073405	1958-2007	350-690	43	106.14	109.12	94.24	502.35	7.94
JL-4905-601	36A	31.95697	-106.4073405	n/a	n/a	n/a	n/a	n/a	n/a	1128	n/a
JL_4905-607	40	31.92802	-106.3912856	1959-2005	308-826	23.06	74.98	57.67	52.31	324.7	8.11
JL-4905-637	40A	31.92802	-106.3912856	1999-2013	650-885	31.87	84.27	102.27	42.67	366.67	7.47
JL-4905-204	41	31.97151	-106.4246224	1959-2005	359-515	34.39	127.9	132.43	79.86	507.35	7.94
JL-4905-301	42	31.97185	-106.4095069	1958-2007	320-671	31.19	85.48	84.83	51.14	375.07	8.05

JL-4905-301	42	31.97185	-106.4095069	1958-2007	320-671	31.19	85.48	84.83	51.14	375.07	8.05
JL-4905-605	44	31.9426	-106.3782061	1960-2013	324-769	41.25	100.13	208.08	46.7	440.03	8.06
JL-4905-605	44	31.9426	-106.3782061	1960-2013	324-769	41.25	100.13	208.08	46.7	440.03	8.06
JL-4905-903	51	31.91492	-106.3954912	1963-2013	269-1037	26.8	88.86	68.6	63.92	382	8.04
JL-4905-903	51	31.91492	-106.3954912	1963-2013	269-1037	26.8	88.86	68.6	63.92	382	8.04
JL-4905-903	51	31.91492	-106.3954912	1963-2013	269-1037	26.8	88.86	68.6	63.92	382	8.04
JL-4905-504	52	31.9287	-106.4431667	1961-2013	481-1152	44.5	54.26	25.68	49.94	357.24	7.72
JL-4905-504	52	31.9287	-106.4431667	1961-2013	481-1152	44.5	54.26	25.68	49.94	357.24	7.72
JL-4905-504	52	31.9287	-106.4431667	1961-2013	481-1152	44.5	54.26	25.68	49.94	357.24	7.72
JL-4905-303	53	31.97583	-106.3960251	1955-2000	380-860	78.17	229.2	447.03	52.73	909.67	7.91
JL-4905-303	53	31.97583	-106.3960251	1955-2000	380-860	78.17	229.2	447.03	52.73	909.67	7.91
JL-4905-304	54	31.97587	-106.3873375	1955-1974	377-746	77.94	276.25	523.94	58.06	1066.69	7.88
JL-4905-304	54	31.97587	-106.3873375	1955-1974	377-746	77.94	276.25	523.94	58.06	1066.69	7.88
JL-4906-101	57	31.97149	-106.3581841	1965	n/a	115.6	245.8	465	151.2	1060.2	7.54
JL-4905-214	58	31.9826	-106.4250553	1996-2006	276-685	58.64	145.1	211.1	102.13	632	7.9
JL-4905-214	58	31.9826	-106.4250553	1996-2006	276-685	58.64	145.1	211.1	102.13	632	7.9
JL-4906-401	59	31.95684	-106.3622977	1965-2010	348-451	80.42	137.67	274.56	93.58	718.89	7.81
JL-4905-306	61	31.98328	-106.4002868	2000-2006	391-603	89.67	186.67	345.17	109.29	972.83	7.82
JL-4905-306	61	31.98328	-106.4002868	2000-2006	391-603	89.67	186.67	345.17	109.29	972.83	7.82
JL-4905-906	62	31.91386	-106.3795951	1966-2007	330-950	29.18	80.16	98.72	31.34	352.12	8.07
JL-4905-906	62	31.91386	-106.3795951	1966-2007	330-950	29.18	80.16	98.72	31.34	352.12	8.07
JL-4905-906	62	31.91386	-106.3795951	1966-2007	330-950	29.18	80.16	98.72	31.34	352.12	8.07
JL-4905-914	516	31.88643	-106.4012598	1992-2012	371-935	27.26	102.64	98.87	72.37	390.19	7.93
JL-4905-914	516	31.88643	-106.4012598	1992-2012	371-935	27.26	102.64	98.87	72.37	390.19	7.93
JL-4905-914	516	31.88643	-106.4012598	1992-2012	371-935	27.26	102.64	98.87	72.37	390.19	7.93
JL-4905-635	521	31.92923	-106.3753919	1992-2011	380-965	57.66	139.23	293.62	26.2	629.31	7.89
JL-4905-635	521	31.92923	-106.3753919	1992-2011	380-965	57.66	139.23	293.62	26.2	629.31	7.89
JL-4905-635	521	31.92923	106.3753919	1992-2011	380-965	57.66	139.23	293.62	26.2	629.31	7.89
JL-4905-921	522	31.90691	-106.384787	2005-2012	550-1020	25.55	78.18	108.08	32.16	361.75	8.06
JL-4905-921	522	31.90691	-106.384787	2005-2012	550-1020	25.55	78.18	108.08	32.16	444	8.06

JL-4905-921	522	31.90691	-106.384787	2005-2012	550-1020	25.55	78.18	108.08	32.16	361.75	8.06
n/a	529	31.92271	-106.3975305	n/a	n/a	24.63	78.85	90.43	35.85	332.5	7.98
JL-4905-922	601	31.89833	-106.382833	2005-2010	700-931	24.63	78.85	90.43	35.85	328	7.98
JL-4905-922	601	31.89833	-106.382833	n/a	n/a	24.63	78.85	90.43	35.85	332.5	7.98
n/a	FBT 10	31.89423	-106.3262368	n/a	n/a	n/a	n/a	n/a	n/a	1146	n/a
n/a	FBT 10	31.89423	-106.3262368	n/a	n/a	n/a	n/a	n/a	n/a	1481	n/a
n/a	FBT 05	31.94079	-106.2862043	n/a	n/a	n/a	n/a	n/a	n/a	1207	n/a
n/a	FBT 05	31.94079	-106.2862043	n/a	n/a	n/a	n/a	n/a	n/a	1469	n/a
n/a	FBT 05	31.94079	-106.2862043	n/a	n/a	n/a	n/a	n/a	n/a	1731	n/a
n/a	FBT 04	31.92781	-106.338157	n/a	n/a	n/a	n/a	n/a	n/a	3954	n/a
n/a	MNS T02	31.95845	-106.378051	n/a	n/a	n/a	n/a	n/a	n/a	953	n/a
n/a	MNS T02	31.95845	-106.378051	n/a	n/a	n/a	n/a	n/a	n/a	1311	n/a
n/a	MNS T02	31.95845	-106.378051	n/a	n/a	n/a	n/a	n/a	n/a	2127	n/a
n/a	MNS T03	31.96659	-106.390805	n/a	n/a	n/a	n/a	n/a	n/a	940	n/a
n/a	MNS T03	31.96659	-106.390805	n/a	n/a	n/a	n/a	n/a	n/a	986	n/a
n/a	MNS T03	31.96659	-106.390805	n/a	n/a	n/a	n/a	n/a	n/a	2340	n/a
n/a	MNS T06	31.99518	-106.385088	n/a	n/a	n/a	n/a	n/a	n/a	3905	n/a
n/a	MNS T06	31.99518	-106.385088	n/a	n/a	n/a	n/a	n/a	n/a	3412	n/a
n/a	MNS T06	31.99518	-106.385088	n/a	n/a	n/a	n/a	n/a	n/a	12078	n/a
n/a	MNS T05	31.94249	-106.368275	n/a	n/a	n/a	n/a	n/a	n/a	930	n/a
n/a	MNS T05	31.94249	-106.368275	n/a	n/a	n/a	n/a	n/a	n/a	875	n/a
n/a	MNS T05	31.94249	-106.368275	n/a	n/a	n/a	n/a	n/a	n/a	1219	n/a
n/a	NH1	31.9508	-106.449208	n/a	n/a	n/a	n/a	n/a	n/a	2389	n/a

n/a	NH1	31.9508	-106.449208	n/a	n/a	n/a	n/a	n/a	n/a	3174	n/a
n/a	NH2	31.95773	-106.430704	n/a	n/a	n/a	n/a	n/a	n/a	5501	n/a
n/a	NH2	31.95773	-106.430704	n/a	n/a	n/a	n/a	n/a	n/a	10562	n/a

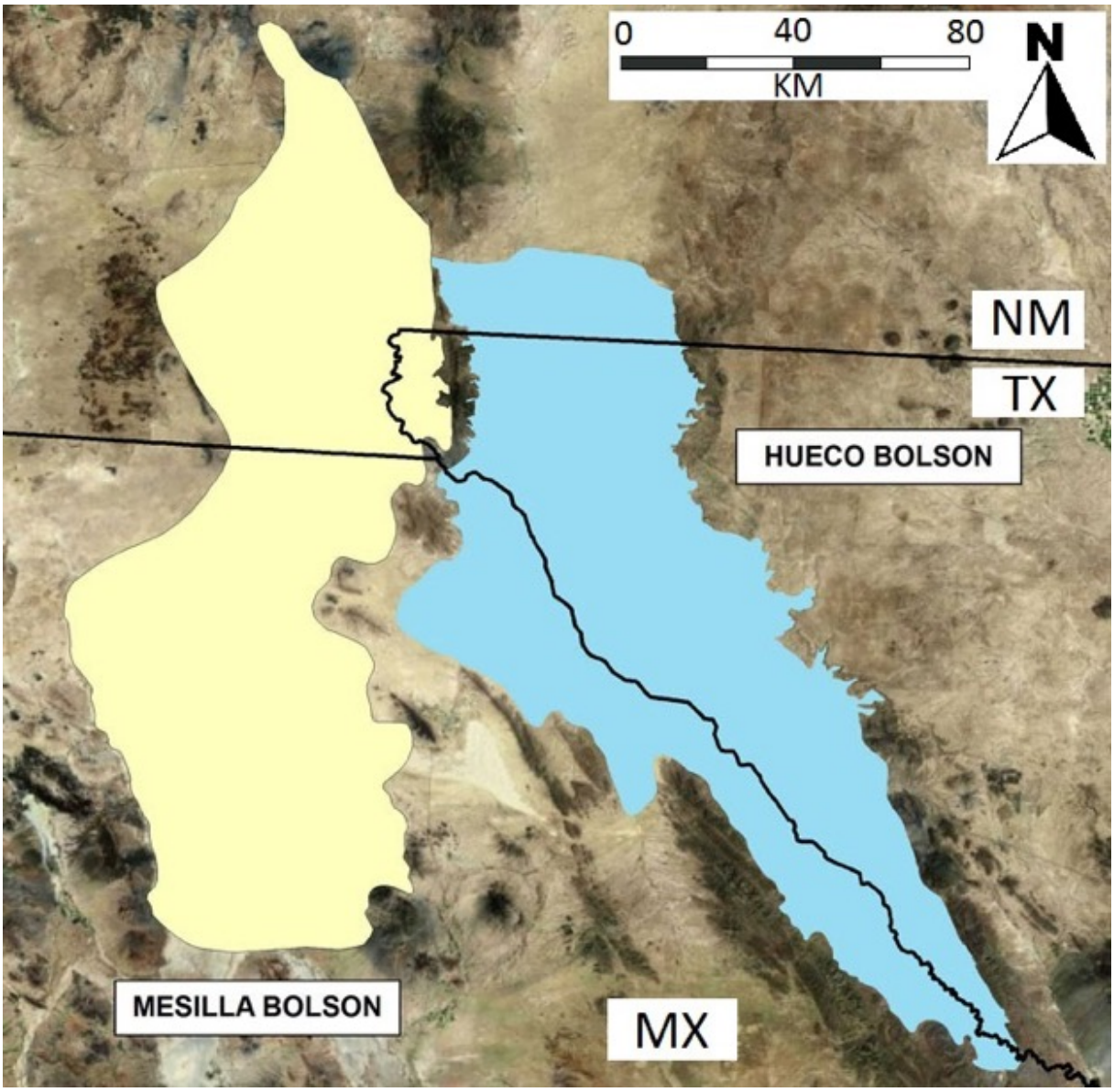

Figure 1

Image modified from El Paso Water Utilities
(https://www.epwater.org/our_water/water_resources/our_aquifers)
Showing extent of the Hueco bolson (blue) and the Mesilla bolson (yellow).

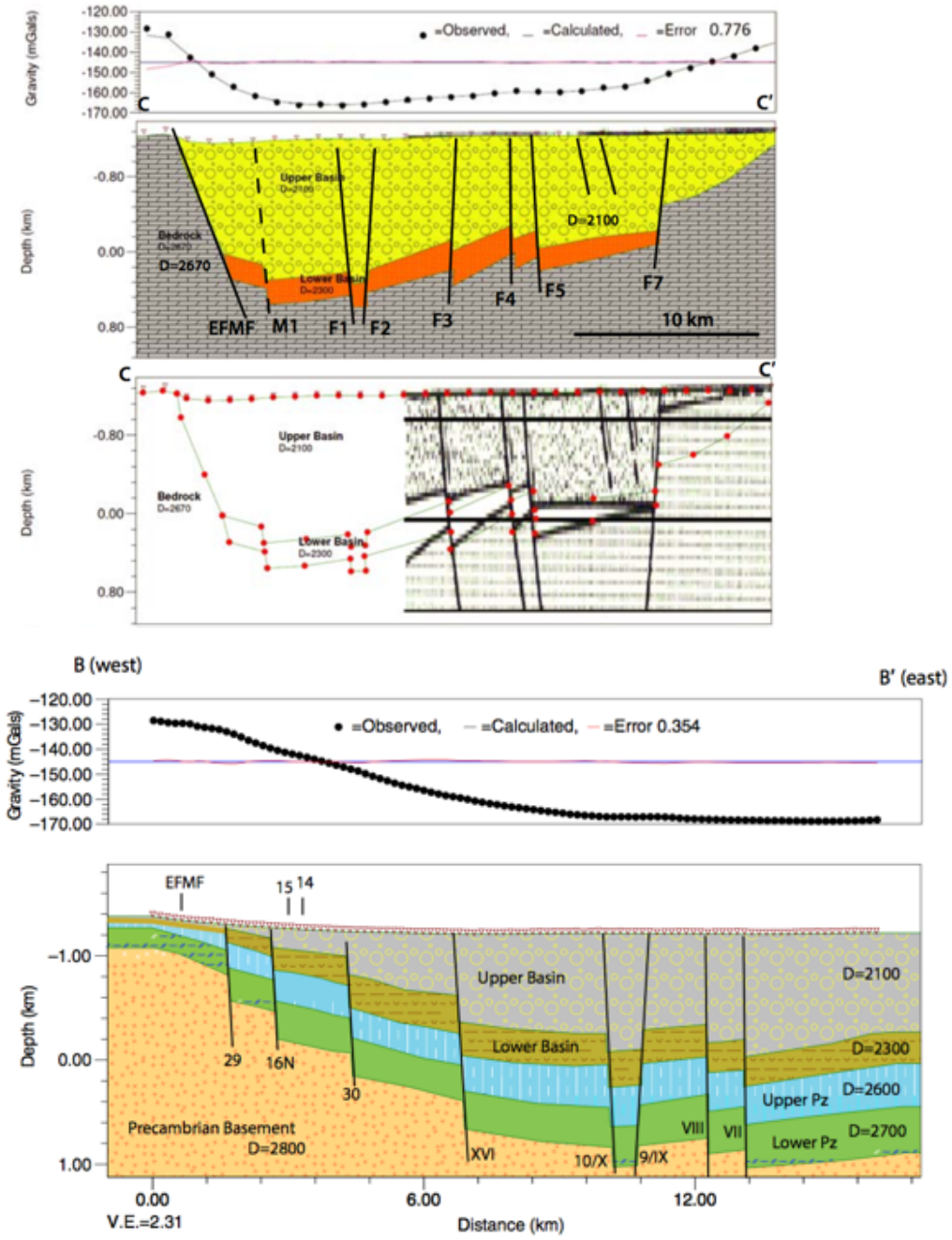

Figure 2

Density profiles C-C' from Avila et al. (2016) and B-B' Budhathoki (2016). These profiles were used to help constrain the density profiles created in this study. The lithology of Avila et al. (2016) was used in this study. "D" values are densities in kg/m^3.

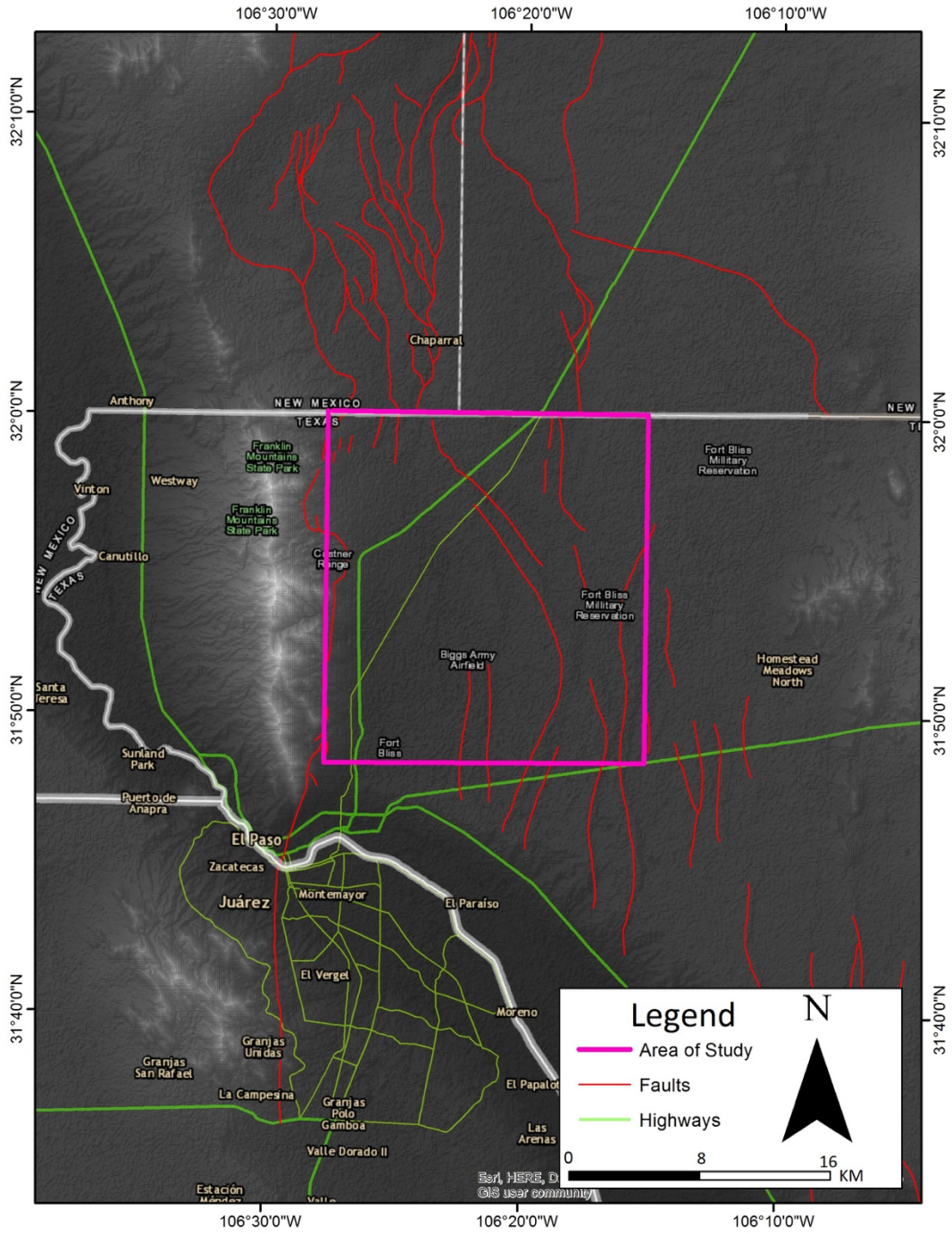

Figure 3

Regional map highlighting study area (pink square). Red lines are Quaternary faults (US Geological Survey, 2018) and green lines represent major highways,

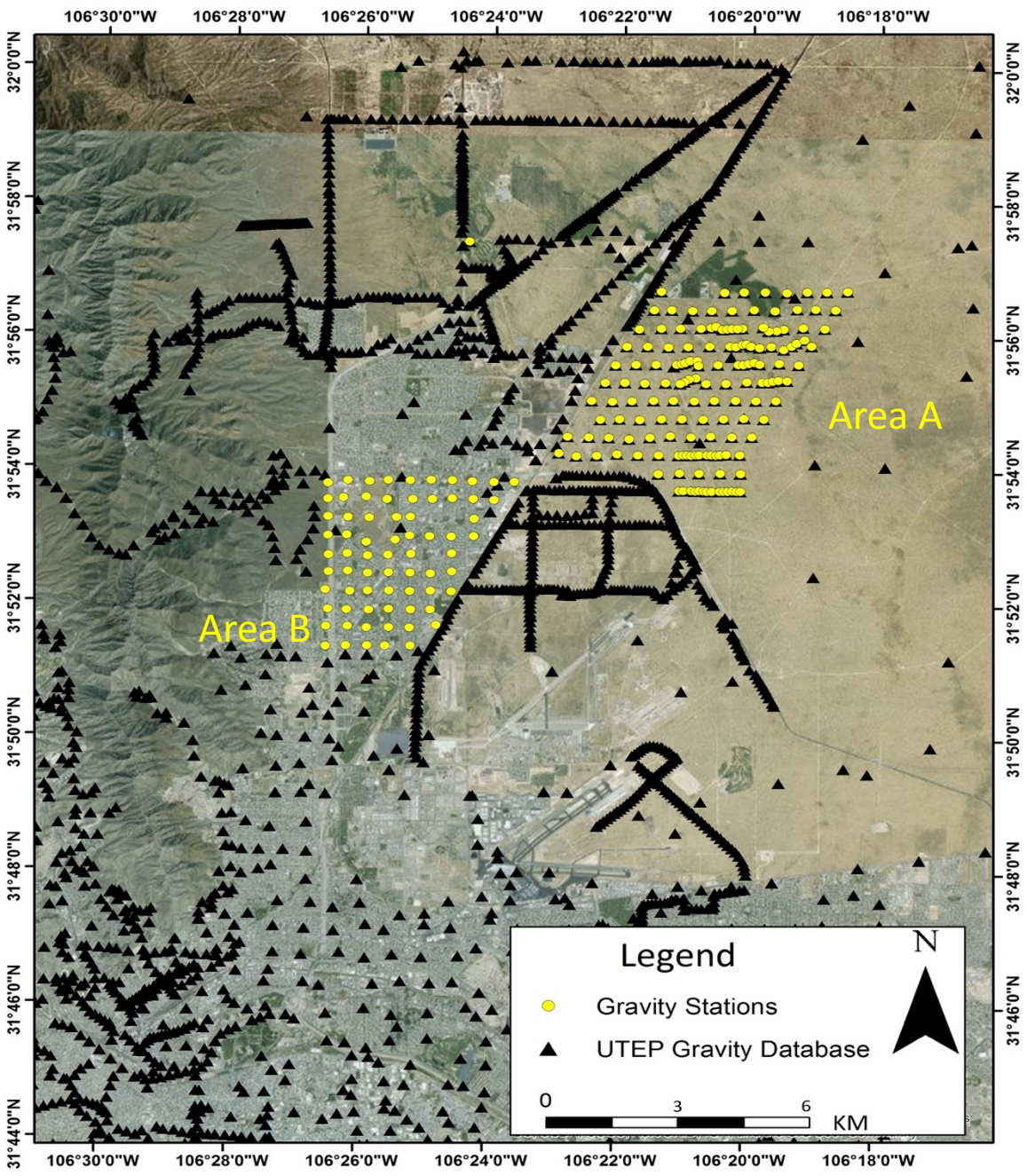

Figure 4

Previous gravity stations within the UTEP Gravity database are indicated by black triangles. New data points collected in study areas are indicated by yellow dots. Area A is located to the northeast within Fort Bliss and Area B is located to the southwest within an urbanized area of El Paso.

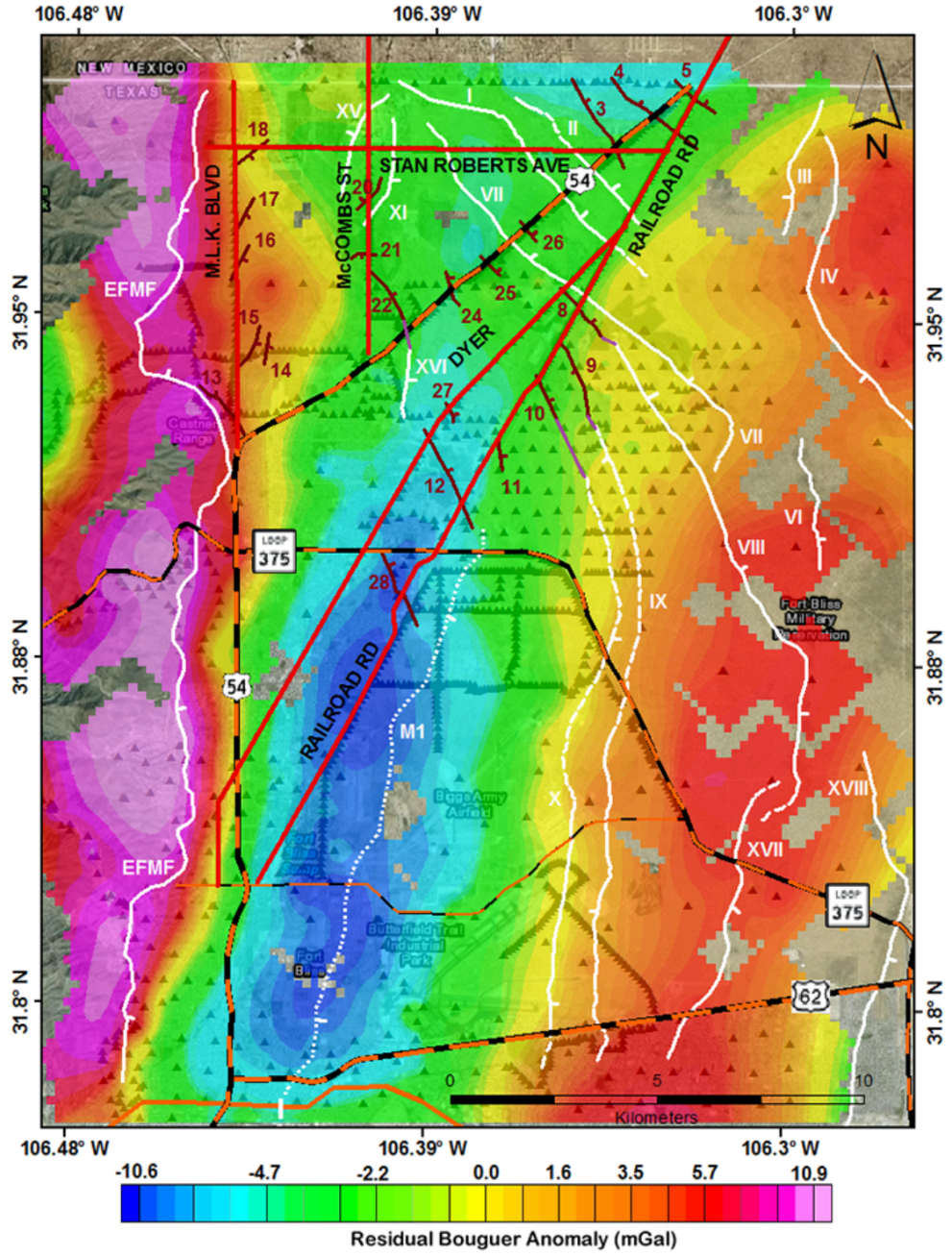

Figure 5

Residual Bouguer anomaly map from Budhathoki et al. (2018). White solid lines with Roman numerals are faults mapped by Collins and Raney (2000). Fault M1, illustrated by a dashed white line, was mapped by Marrufo (2011) and Avila et al. (2016) based on gravity and well-log studies. Brown lines labeled with Arabic numerals are faults suggested by the analysis of simple Bouguer anomalies by Budhathoki et al. (2018). Purple lines denote connections that Budhathoki et al. believe exist between mapped surface faults and faults detected by simple Bouguer anomaly analysis.

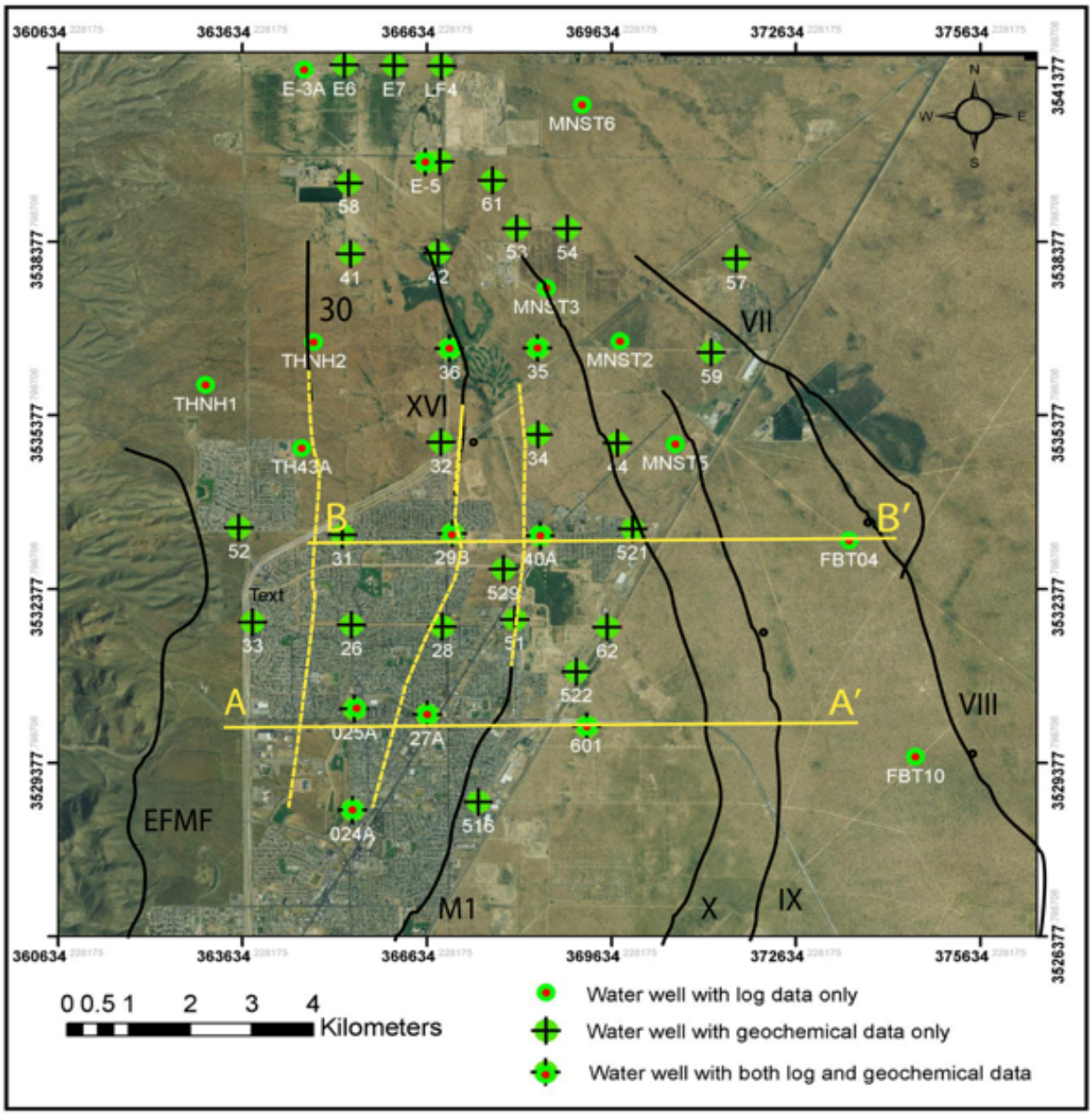

Figure 6

Figure modified from Thapalia (2014) displaying well locations and additional information associated with each individual well. Green dot with black cross indicates log data only, red dot indicates geochemical data only and wells with both a black cross and a red dot indicate wells with log and geochemical data. Black lines represent faults mapped in the area by Avila (2014) Budhathoki (2013), Marrufo (2011), Collins and Raney (1994). See Table 1 for well information.

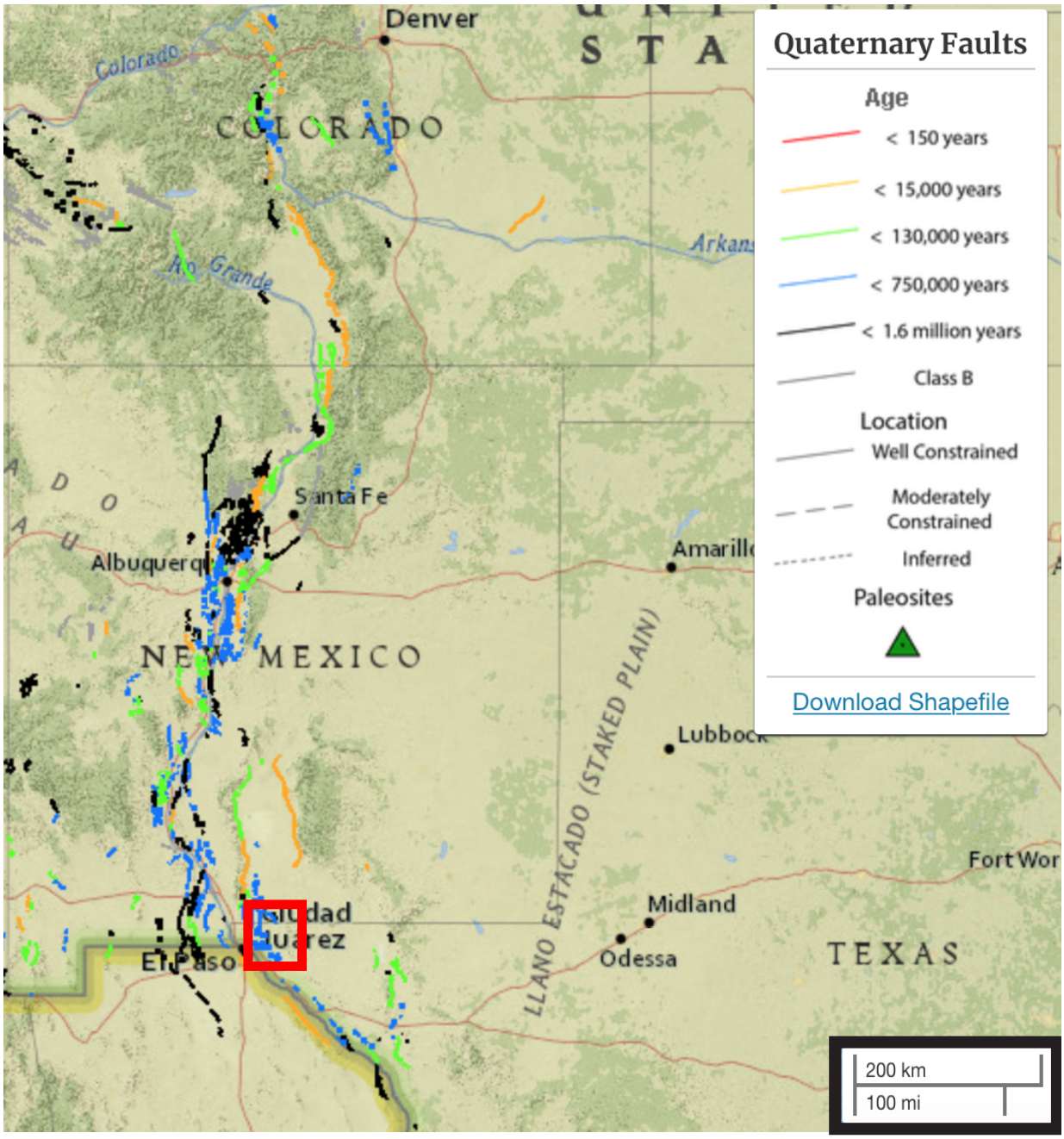

Figure 7

Quaternary faults from the US Geological Survey (2018) showing the extent of the Rio Grande rift from northern Chihuahua, Mexico to central Colorado. The Hueco Bolson is part of a series of interconnected grabens which forms part of the Rio Grande rift system at the US-Mexico border. Red box indicates study area.

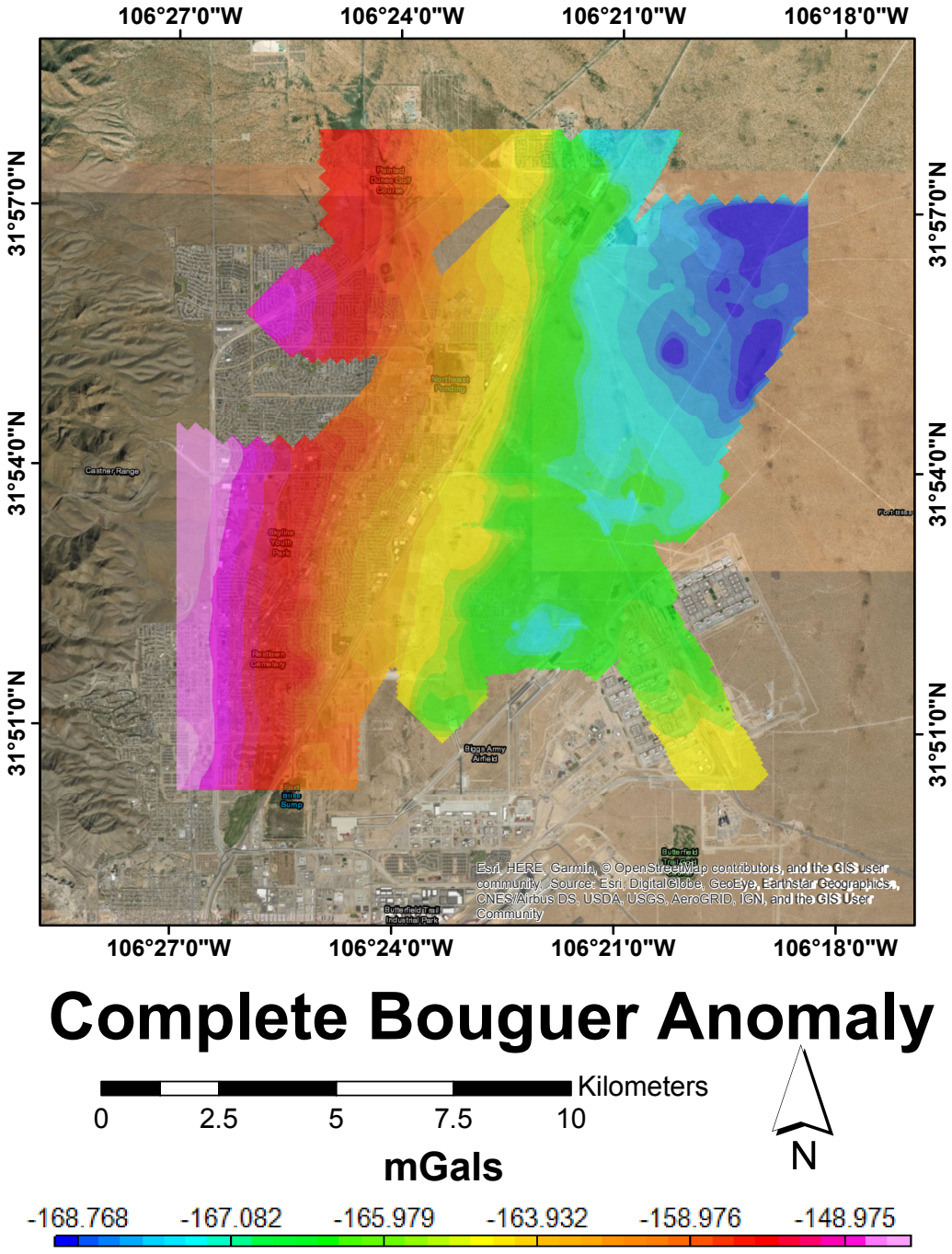

Figure 8

Local complete Bouguer anomaly map of study area. Reducing density of 2670 kg/m^3 was used.

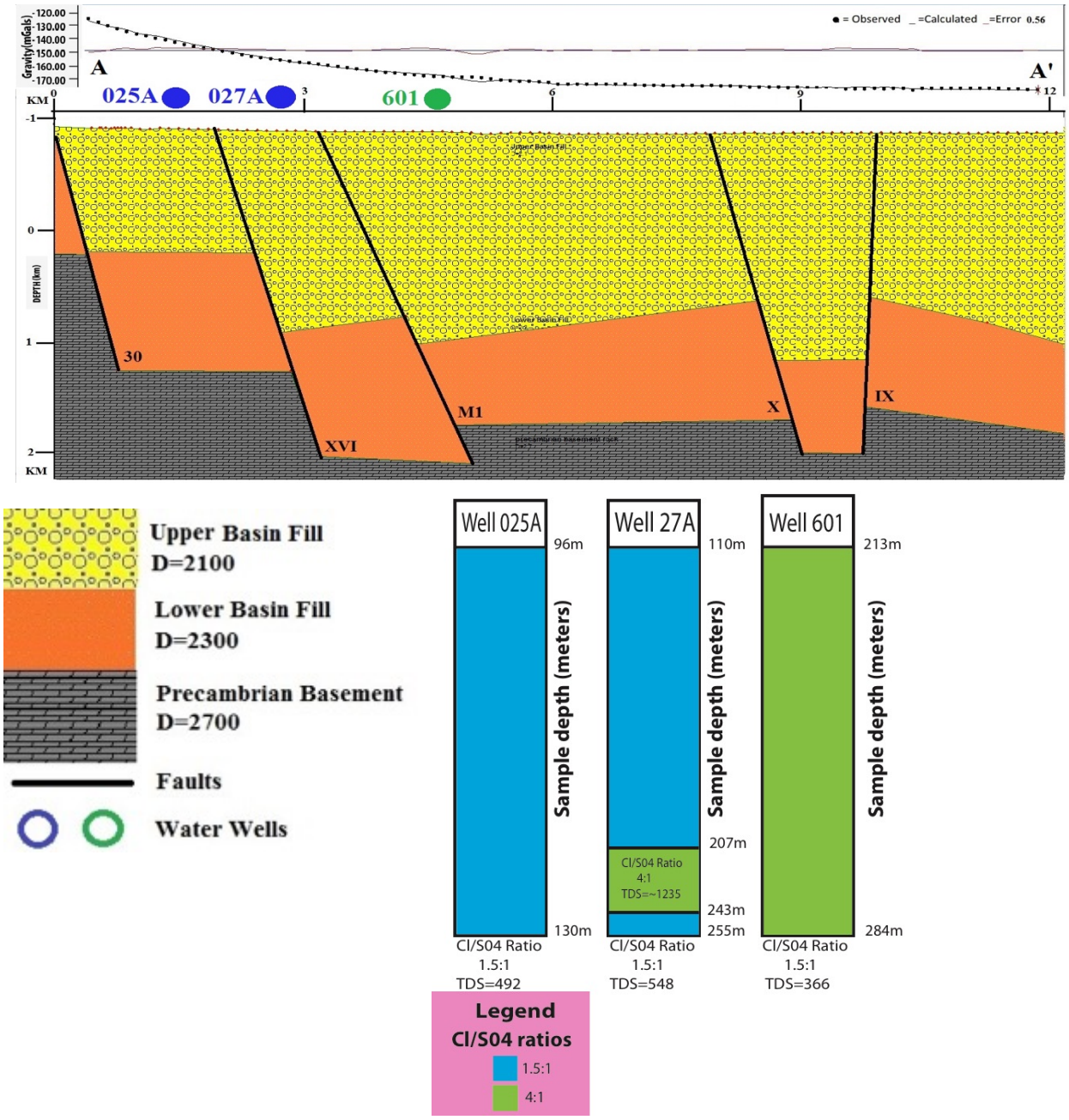

Figure 9

Density Profile A-A' (west to east) is a two-dimensional gravity profile located south of density profile B-B' that was created using a 3-layer model. Faults are solid black lines. Well locations are shown above the density models. The water quality, based on Cl/SO_4 ratios, is shown below the density profile. Depths of intervals sampled are indicated. See Table 1 for more details.

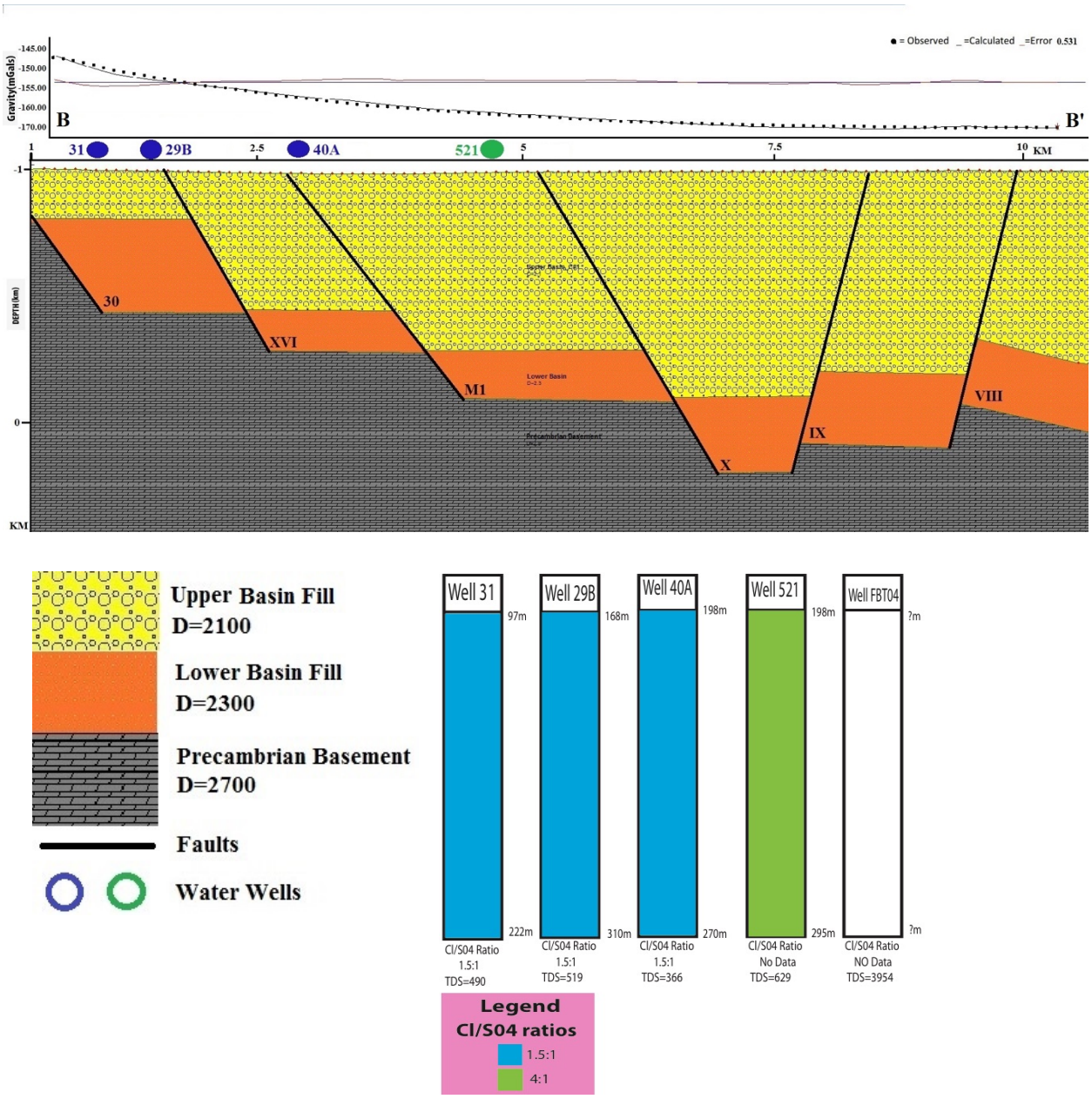

Figure 10

Density Profile B-B' (west to east) is a two-dimensional gravity profile located north of Density Profile A-A''. Created using 3 density layer, faults are solid black lines. Above the density model are labeled well locations which are color coded to the water quality based on Cl/SO_4 ratios. The same is seen in the bar graph, which shows sampling depth ranges over which the ratios were calculated. Thalpia (2014)

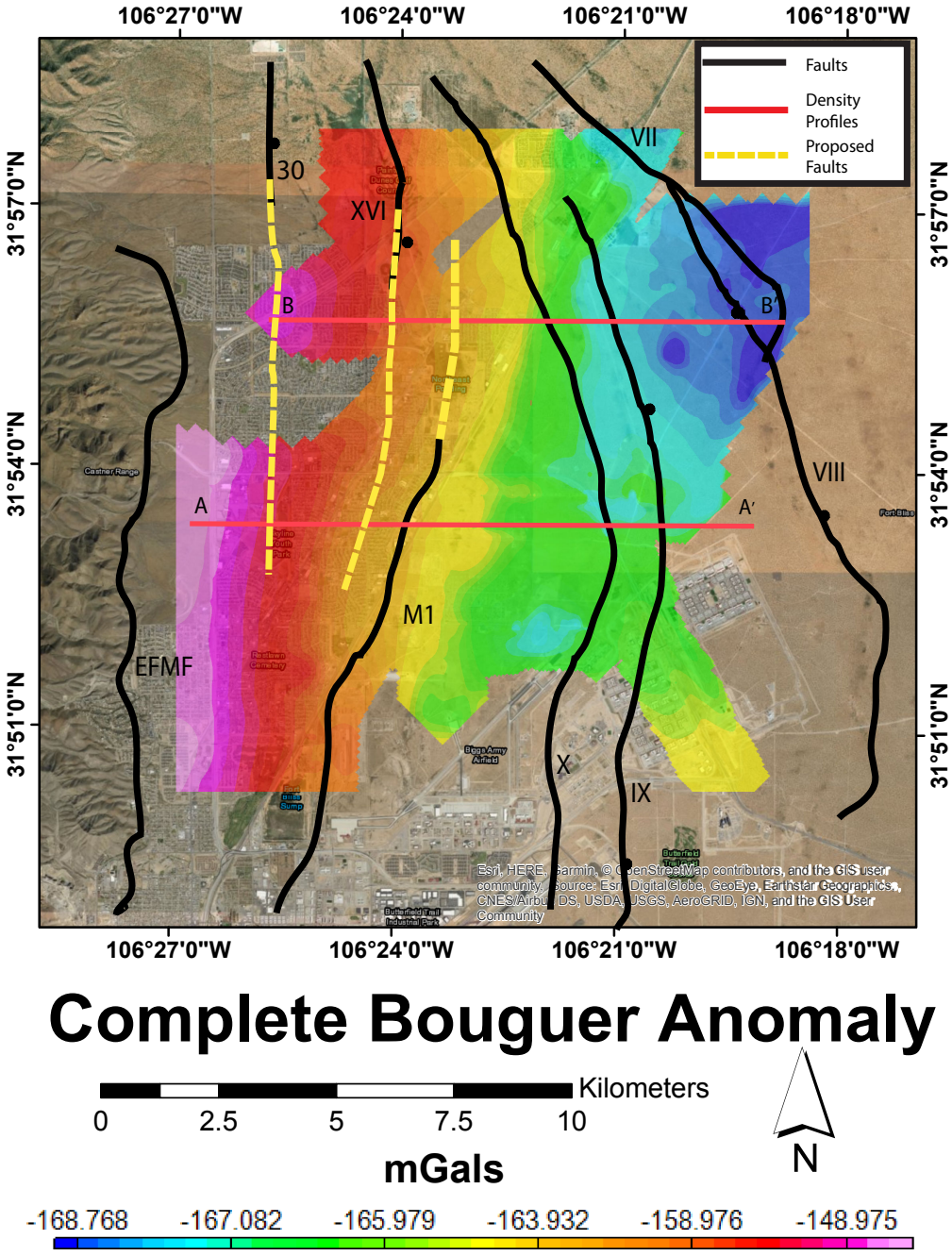

Figure 11

Local complete Bouguer Anomaly Map with faults mapped by Hawley et al. (2009), Marrufo (2011), Budhathoki (2013) and Avila et al. (2016) indicated by black lines. Yellow dashed lines display the faults I extended in the area based on the gravity analysis. The red lines display locations for density profiles A-A' and B-B'

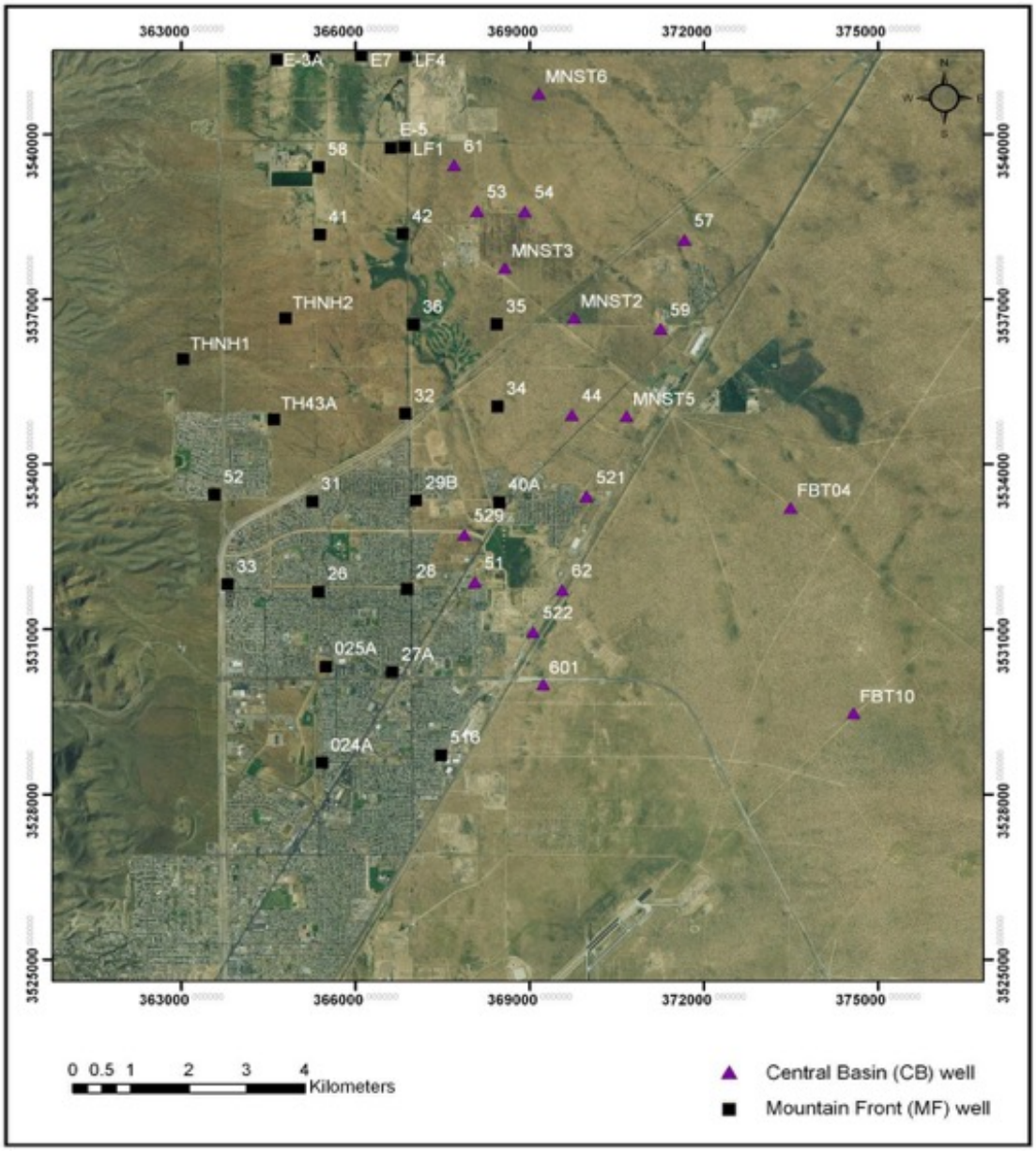

Figure 12

Classification of MF and CB wells of the study area based on the TDS values. Figure modified from Thapalia (2014).

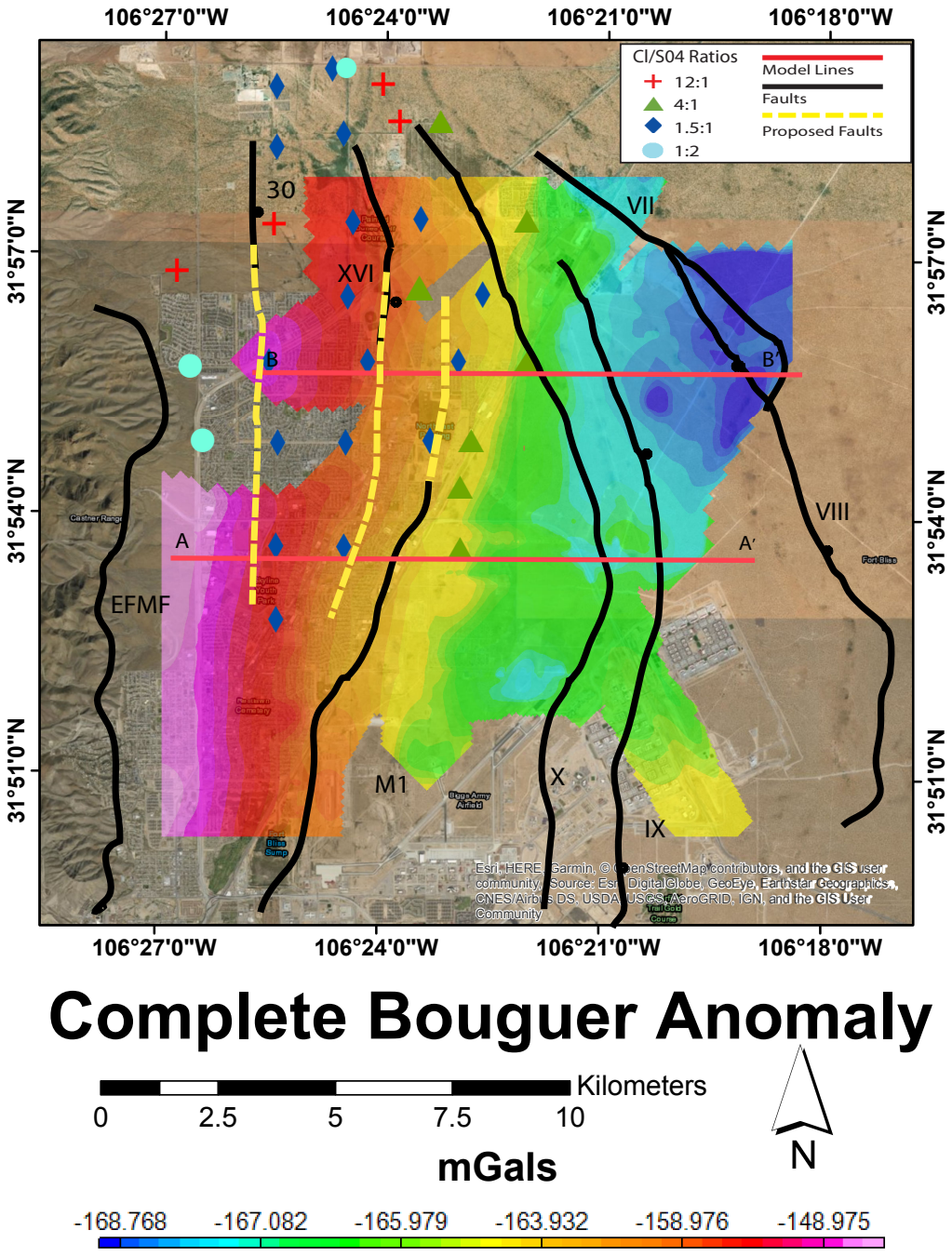

Figure 13

Local complete Bouguer anomaly map with faults mapped by Hawley et al. (2009), Marrufo (2011), Budhathoki (2013), Budhathoki et al. (2018) and Avila et al. (2016) in black lines. Yellow dashed lines display the faults I extended in the area based on the gravity analysis. The red lines display locations of the density profiles A-A' and B-B'. Varying shapes represent well locations as well as water quality depending on the Cl/SO_4ratios calculated by Thapalia (2014)

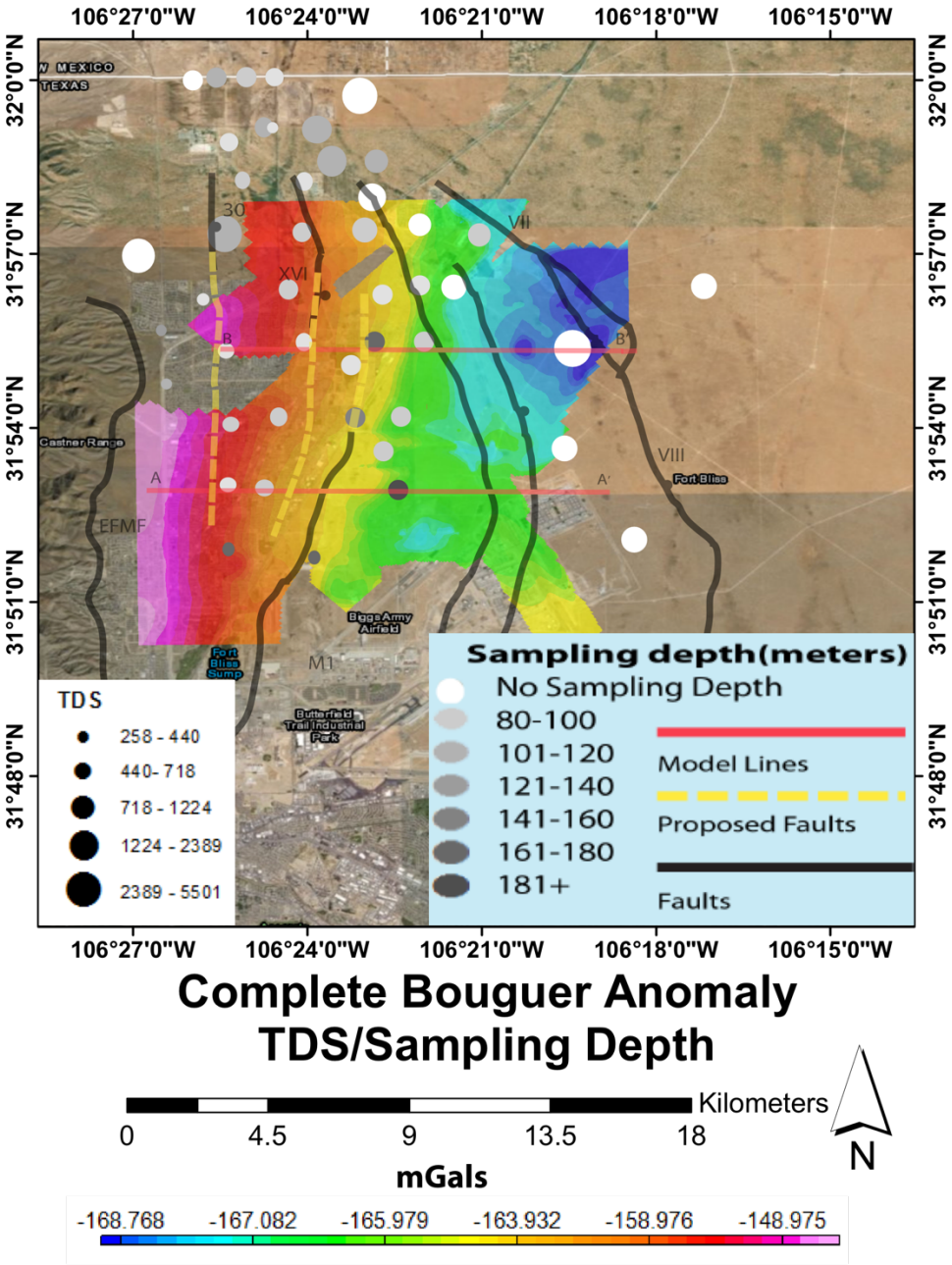

Figure 14

Local complete Bouguer anomaly map displaying faults mapped by Hawley et al. (2009), Marrufo (2011), Budhathoki (2013), Budhathoki et al. (2018) and Avila et al. (2016) in black lines. Yellow dashed lines display the faults I extended in the area based on the gravity analysis. The red lines display locations of density profiles A-A' and B-B'. Circles represent well location, size of symbols related to TDS value as indicated. Colors represent sampling depths. Darker shades of gray are deeper depths as indicated by color bar. White symbols are from wells where details of sampling depths were not available. Data from Thapalia (2014). See Table 1

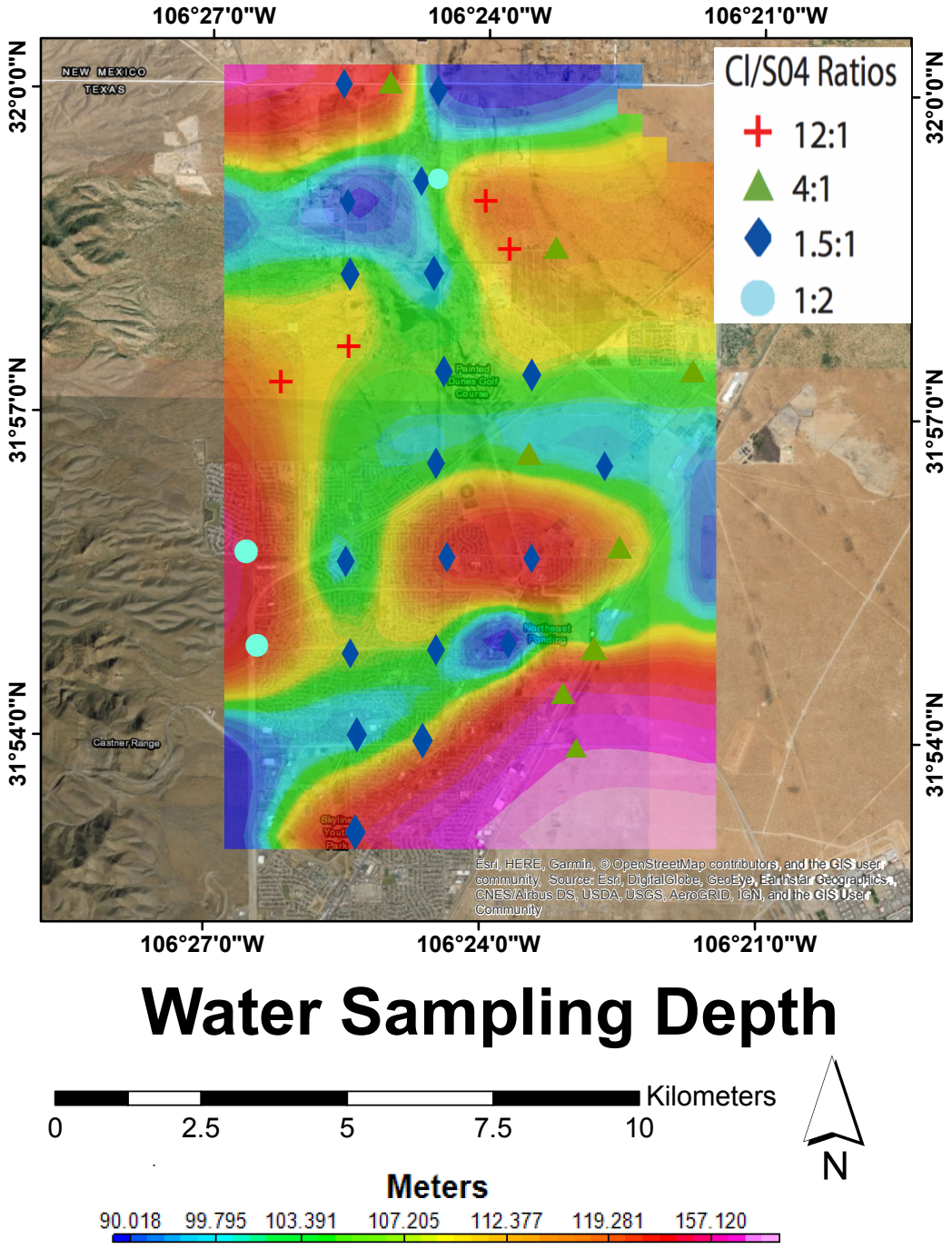

Figure 15

Water sampling depth contour map indicating the top depths of the intervals at which the Cl/SO_4 ratios and top TDS value were measured based on Thapalia (2014).

Vita

Mark Andrew Ornelas was born and raised in El Paso Texas. He obtained his bachelor's degree in Geological Sciences from the University of Texas at El Paso in 2015. After graduation, he continued his graduate studies at the University of Texas at El Paso where he obtained his Master's of Science in Geophysics in December 2018. Mark served as an active member of the Society of Exploration Geophysicist and in the Society of Economic Geology. He was active within the department helping organize events such as as earth science day, Department Colloquium. He traveled to Toronto Canada in March of 2017 to represent UTEP and the Center for Entrepreneurial Geological sciences at PDAC Prospectors and Developer's Association of Canada. He also traveled to Lima Peru in May of 2017 to present a short course at the PROEXPLO along with other members and professors of CEGS.

Marc worked fulltime as a wellsite geologist and utilities mapping specialist during his graduate studies gaining invaluable experience, as his professional and academic career grew. He plans to continue as a utilities mapping specialist in the near future.

Contact Information: Mark Andrew Ornelas

marcornelas1003@gmail.com

This thesis was typed by Mark Andrew Ornelas